# ENVISAT GOMOS Monthly report: April 2004

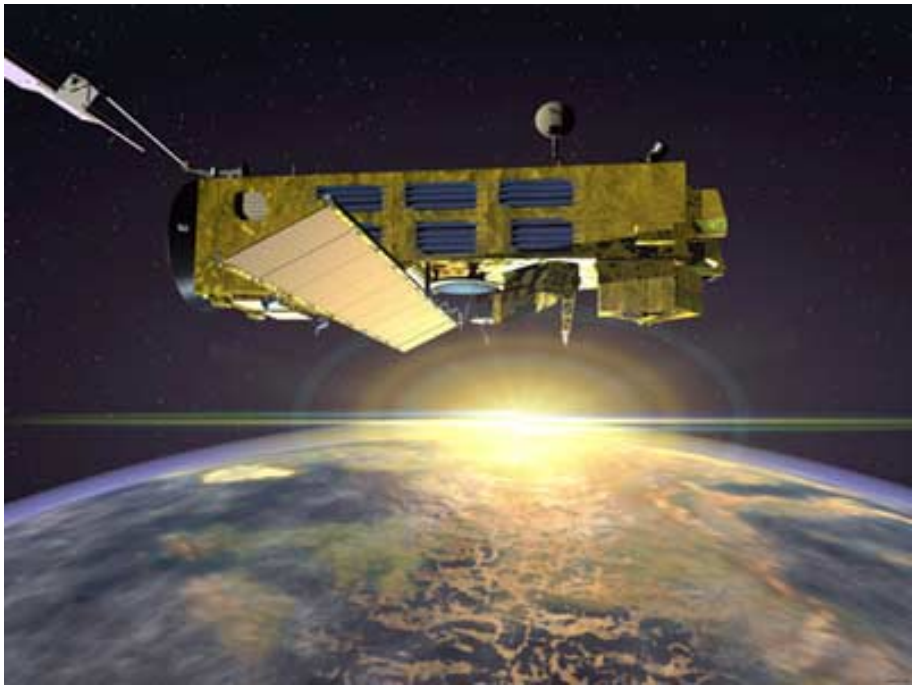

| | | |
|---|---|---|
| Prepared by: | PCF Team | ESA EOP-GOQ |
| Inputs from: | GOMOS Quality Working Group | |
| Issue: | 1.0 | |
| Reference: | ENVI-SPPA-EOPG-TN-04-0016 | |
| Date of issue: | 10 June 2004 | |
| Status: | Reviewed | |
| Document type: | Technical Note | |
| Approved by: | Pascal Lecomte, Rob Koopman | |

# TABLE OF CONTENTS

# 1 INTRODUCTION

The GOMOS monthly report documents the current status and recent changes to the GOMOS instrument, its data processing chain, and its data products.
The Monthly Report (hereafter MR) is composed of analysis results obtained by the Product Control Facility, combined with inputs received from the different entities working on GOMOS operation, calibration, product validation and data quality. These teams participate in the GOMOS Quality Working Group:

- European Space Agency (ESRIN-PCF, ESOC, ESTEC-PLSO)
- ACRI
- Service d'Aeronomie
- Finnish Meteorological Institute
- IASB-Belgian Institute for Space Aeronomy
- Astrium Space
- ECMWF

In addition, the group interfaces with the Atmospheric Chemistry Validation Team.

## *1.1 Scope*

The main objective of the Monthly Report is to give, on a regular basis, the status of GOMOS instrument performance, data acquisition, results of anomaly investigations, calibration activities and validation campaigns. The following six sections compose the MR:

- Summary
- Unavailability
- Instrument Performance and Configuration
- Level 1 Product Quality Monitoring
- Level 2 Product Quality Monitoring
- Validation Activities and Results

## *1.2 References*

[1] ENVISAT Weekly Mission Operations Report #95, #96, #97, #98, #99 ENVI-ESOC-OPS-RP-1011-TOS-OF
[2] 'Level 1b Detailed Processing Model', PO-RS-ACR-GS-0001, issue 6.1, 28 Nov, 2003
[3] 'Level 2 Detailed Processing Model', PO-RS-ACR-GS-0002, issue 6.0, 6 Feb, 2004

## *1.3 Acronyms and Abbreviations*

ACVT Atmospheric Chemistry Validation Team
ADF Auxiliary Data File

| | |
|---|---|
| ADS | Auxiliary Data Server |
| ANX | Ascending Node Crossing |
| ARF | Archiving Facility (PDS) |
| CCU | Central Communication Unit |
| CFS | CCU Flight Software |
| CNES | Centre National d'Études Spatiales |
| CTI | Configuration Table Interface / Configurable Transfer Item |
| CR | Cyclic Report |
| DC | Dark Charge |
| DMOP | Detailed Mission Operation Plan |
| DPM | Detailed Processing Model |
| DS | Data Server |
| DSA | Dark Sky Area |
| DSD | Data Set Descriptor |
| ECMWF | European Centre for Medium Weather Forecast |
| EQSOL | Equipment Switch Off Line |
| ESA | European Space Agency |
| ESL | Expert Support Laboratory |
| ESRIN | European Space Research Institute |
| ESTEC | European Space Research & Technology Centre |
| ESOC | European Space Operations Centre |
| FCM | Fine Control Mode |
| FMI | Finnish Meteorological Institute |
| FOCC | Flight Operations Control Centre (ENVISAT) |
| FP1 | Fast Photometer 1 |
| FP2 | Fast Photometer 2 |
| GADS | Global Annotations Data Set |
| GOMOS | Global Ozone Monitoring by Occultation of Stars |
| GOPR | GOmos PRototype |
| GS | Ground Segment |
| HK | Housekeeping |
| IASB | Institut d'Aeronomie Spatiale de Belgique |
| IAT | Interactive Analysis Tool |
| ICU | Instrument Control Unit |
| IDL | Interactive Data Language |
| IECF | Instrument Engineering and Calibration Facilities |
| IMK | Institute of Meteorology Karlsruhe (Meteorologisch Institut Karlsuhe) |
| INV | Inventory Facilities (PDS) |
| IPF | Instrument Processing Facilities (PDS) |
| JPL | Jet Propulsion Laboratory |
| LAN | Local Area Network |
| LPCE | Laboratoire de Physique et Chimie de l'Environnement |
| LUT | Look Up Table |
| MCMD | Macro Command |
| MDE | Mechanism Drive Electronics |
| MIP | Most Illuminated Pixel |
| MPH | Main Product Header |
| MPS | Mission Planning System |

| | |
|---|---|
| MR | Monthly Report |
| OBT | On Board Time |
| OCM | Orbit Control Manoeuvre |
| OOP | Out-of-plane |
| OP | Operational Phase of ENVISAT |
| PAC | Processing and Archiving Centre (PDS) |
| PCF | Product Control Facility |
| PDCC | Payload Data Control Centre (PDS) |
| PDHS | Payload Data Handling Station (PDS) |
| PDHS-E | Payload Data Handling Station – ESRIN |
| PDHS-K | Payload Data Handling Station – Kiruna |
| PDS | Payload Data Segment |
| PEB | Payload Equipment Bay |
| PLSOL | Payload Switch off Line |
| PMC | Payload Module Computer |
| PRNU | Pixel Response Non Uniformity |
| PSO | On-Orbit Position |
| QC | Quality Control |
| QUARC | Quality Analysis and Reporting Computer |
| QWG | Quality Working Group |
| RIVM | Rijksinstituut voor Volksgezondheid en Milieu |
| RTS | Random Telegraphic Signal |
| SA | Service d'Aeronomie |
| SAA | South Atlantic Anomaly |
| SATU | Star Acquisition and Tracking Unit |
| SFA | Steering Front Assembly |
| SFCM | Stellar Fine Control Mode |
| SFM | Steering Front Mechanism |
| SMNA | Servicio Meteorológico Nacional de Argentina |
| SODAP | Switch On and Data Acquisition Phase |
| SPA1 | Spectrometer A CCD 1 |
| SPA2 | Spectrometer A CCD 2 |
| SPB1 | Spectrometer B CCD 1 |
| SPB2 | Spectrometer B CCD 2 |
| SPH | Specific Product Header |
| SQADS | Summary Quality Annotation Data Set |
| SSP | Sun Shade Position |
| SZA | Solar Zenith Angle |

# 2 SUMMARY

During the reporting month GOMOS instrument had two planned unavailability periods: on 7th and on 14th April. For the rest of the month, GOMOS has been operating nominally (section 3.1).

The PDS data availability is very high during the month for level 0 products whereas for level 1 there is a decrease during the second week arriving to almost 90% of availability (section 3.3).

The detector temperatures during April are 0.5 degrees higher than the ones registered in March. The expected seasonal variation of the temperatures with amplitude of around one degree can be clearly observed. It can be also observed a small overall temperature increase due to the ageing of the radiators (April 2004 one degree higher than April 2003) (section 4.2).

In the actual processor version (GOMOS/4.02) operational since 23rd March 2004, a Look Up Table (LUT) gives the line index of the star spectra location as a function of the wavelength. A new calibration exercise has been performed during April. The position of the stellar spectra of star id 31, 18 and 4 observed in dark-limb spatial spread monitoring mode have been averaged above 120 km altitude and compared to the values of the LUT. The results confirm the LUT values so for the time being there is no need to update the LUT (section 4.3)

The standard deviation of the modulation signal presents high values after the inclusion, at the end of March, of the ESRIN level 0 data. Although it is to be confirmed, it is suspected that the South Atlantic Anomaly is the cause of these unexpected peaks. The quality of ESRIN data, in particular over the SAA zone, is thus under investigation (section 4.4.2).

The elevation MIP has a significant variation till 12th December 2003 when a new PSO algorithm was activated in order to reduce the deviations of the ENVISAT platform attitude with respect to the nominal one. The amplitude of the MIP displacement seems now to be much smaller confirming that the algorithm is working as expected (section. 4.5.3).

The variation of the radiometric sensitivity ratio is outside the threshold for some photometer ratios and for some stars. ACRI ESL has performed some investigations and two possible causes have been identified up to now: the vignetting correction and an inaccurate reflectivity correction LUT. A new reflectivity correction LUT is in use since 12th February 2004 but some ratios are already outside the threshold and thus more investigations are needed (section 5.4.1).

On 5th, 13th and 22nd April new calibration ADF's were disseminated with updated DC maps of orbits 10974, 11085 and 11215 respectively. This month, also the processing level 1b configuration file (GOM_PR1_AX) has been updated (section 5.1.2)

# 3 INSTRUMENT UNAVAILABILITY

## *3.1 GOMOS Unavailability Periods*

In table 3.1-1 there is a list of GOMOS unavailability reports issued during the period 1st April (00:00:00) until 30th April 2004. Only two planned instrument unavailabilities occurred during the reporting month.

**Table 3.1-1: List of unavailability periods issued during the reporting month**

| Reference of unavailability report | Start time Star orbit | Stop time Stop orbit | Description |
|---|---|---|---|
| EN-UNA-2004/0110 | 7 Apr 2004 18:00:00.000 Orbit = 11003 | 7 Apr 2004 21:21:00.000 Orbit = 11005 | FCM |
| EN-UNA-2004/0111 | 14 Apr 2004 02:45:00.000 Orbit = 11094 | 14 Apr 2004 14:00:00.000 Orbit = 11100 | OCM and MIPAS |

## *3.2 Stars Lost in Centering*

The acquisition of a star initiates with a rallying phase where the telescope mechanism is directed towards the expected position of the star. Subsequently the acquisition procedure enters into detection mode, where the SATU star tracker output signal is pre-processed for spot presence survey and for the location of the most illuminated couple of adjacent pixels for two added lines, over the detection field. The Most Illuminated Pixel (MIP) defines the position of the first SATU centering window. The next step in the acquisition sequence is then initiated and consists of a centering phase where the SATU output signal is pre-processed for spot presence survey over the maximum of 10x10 pixel field. This allows the third phase to begin: the tracking phase.

The centering phase has occasionally resulted in loss of the star from the field of view. The fig. 3.2-1 reports the percentage of the stars lost in centering for the period 03-FEB-2003 to 02-MAY-2004. It can be seen that three stars, mainly weak stars (higher star id means higher magnitude) are lost during centering phase between 4 and 6.5 % of their planned observations. The star id 115 was lost in 40% of the times but it was planned to be occulted five times and was lost twice (in period 26$^{th}$ January – 1$^{st}$ February), so this high percentage of loss is not statistically significant.

As the monitoring shows neither trend nor excessively high percentages of loss, there is no need for the moment to reject any star from the catalogue, and there is no indication of instrument-related problems.

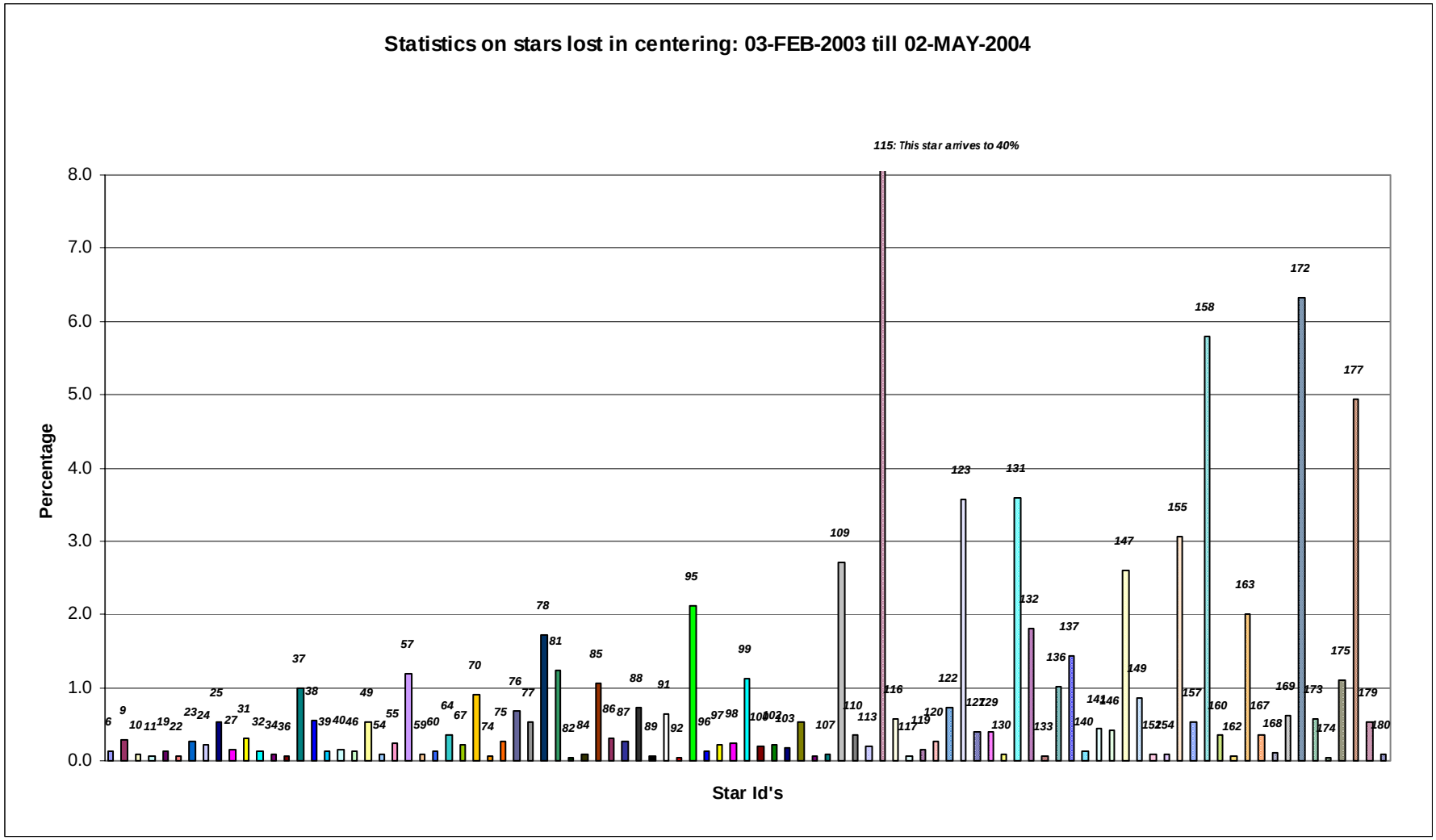


**Figure 3.2-1: Statistics on stars that have been lost during the centering phase. The number above the columns correspond to the Star Id**

## 3.3 Data Generation Gaps

The trend in percentage of available data within the archives PDHS-K and PDH-E is depicted in fig. 3.3-1 (when instrument was in operation). It is a good indicator on how the PDS chain is working in terms of generation and dissemination of data to the archives. The percentage is calculated once per week.

The level 0 availability is very high during the month (almost 100%) whereas for level 1 there is a pronounced decrease during the second week arriving to almost 90% of availability.

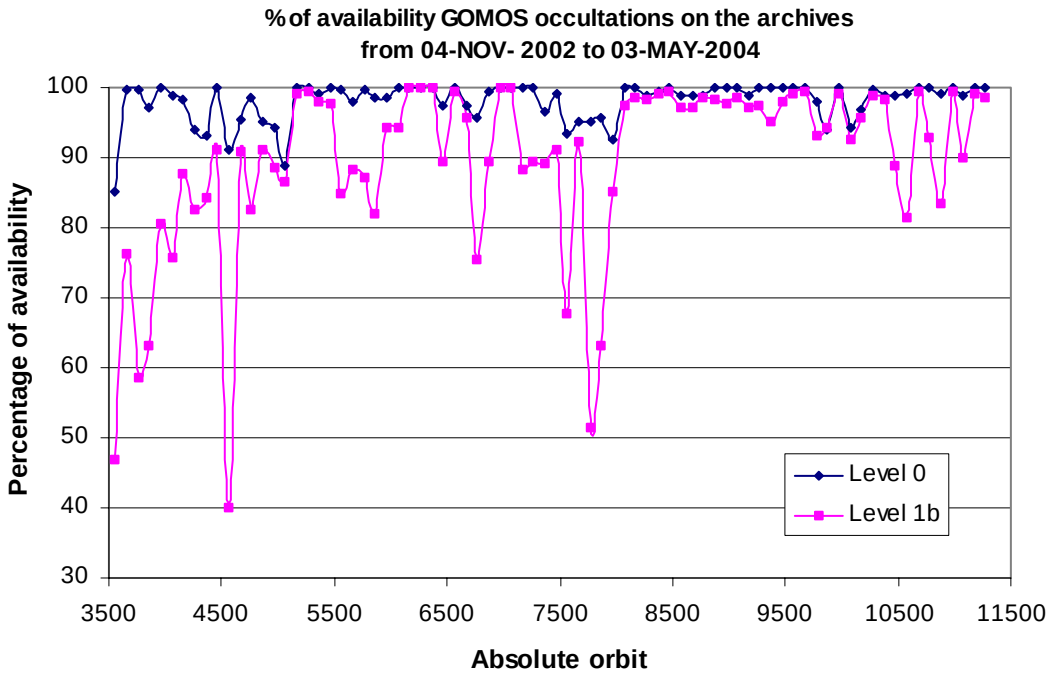


**Figure 3.3-1: Percentage of level 0 and level 1b data availability on the archives PDHS-E and PDHS-K**

### 3.3.1 LEVEL 0 PRODUCTS: GOM_NL__0P

Occultations planned to be acquired but for which no GOM_NL__0P data product has become available are presented in fig. 3.3-2 for the reporting month.

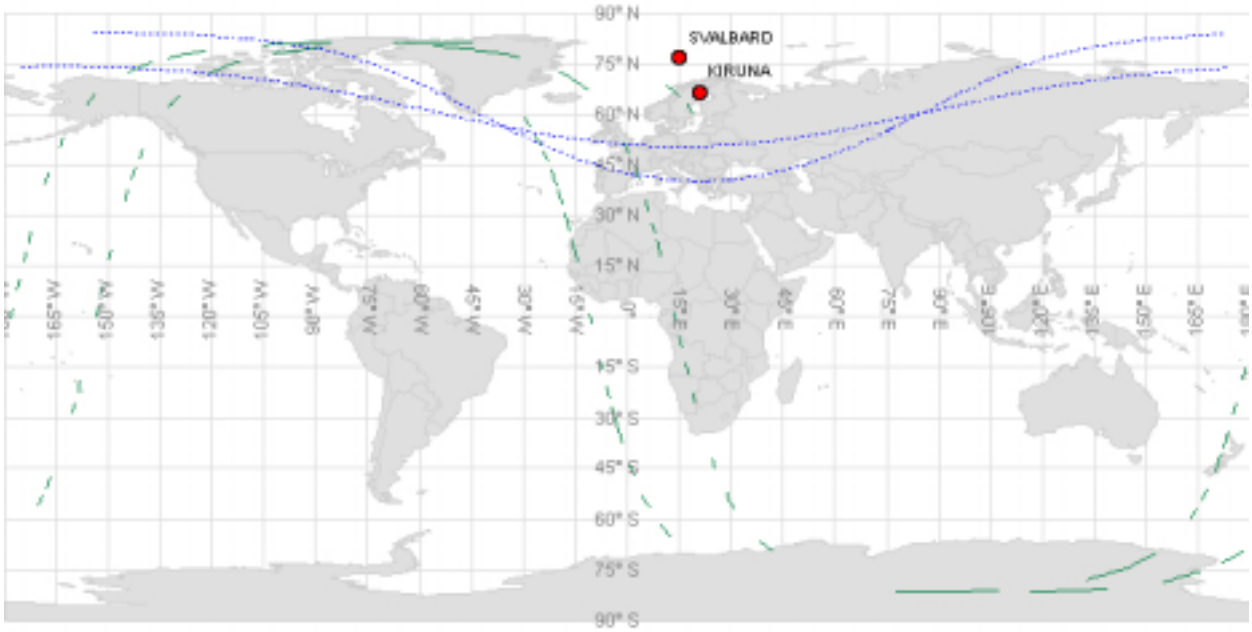


**Figure 3.3-2: The green lines are the orbit segments corresponding to planned data acquisitions for which no GOMOS level 0 product has become available. The blue dashed curve represents the visibility of Kiruna and Svalbard acquisition stations**

### 3.3.2 HIGHER LEVEL PRODUCTS

Routine dissemination of higher-level products produced by the PDS to Cal/Val teams and other users is enabled. Currently ESA provides the Cal/Val teams with selected products that are generated with the prototype processor developed and operated by ACRI.

# 4 INSTRUMENT CONFIGURATION AND PERFORMANCE

## *4.1 Instrument Operation and Configuration*

During the period end of March 2003 to July 2003 the azimuth range had to be decreased in steps (table 4.1-1) to avoid an instrument problem ("Voice_coil_command_saturation" anomaly) that caused GOMOS to go into STAND BY/REFUSE mode. On July 2003 the driver assembly was switched to the redundant B-side and since that date the full azimuth range (-10.8, +90.8) is again available.

**Table 4.1-1: Historical changes in Azimuth configuration**

| Date | Orbit | Minimum Azimuth | Maximum Azimuth |
|---|---|---|---|
| 29-MAR-2003 17:40 | 5635 | 0.0 | +90.8 |
| 31-MAY-2003 06:22 | 6530 | +4.0 | +90.8 |
| 16-JUN-2003 16:17 | 6765 | +12.0 | +90.8 |
| 15-JUL-2003 01:39 | 7200 | -10.8 | +90.8 |

The operations of the instrument in other modes than occultation mode are identified in table 4.1-2.

There was no new Configurable Table Interface (CTI) uploaded to the instrument. The files used since the beginning of the mission are in table 4.1-3.

**Table 4.1-2: GOMOS operations during the reporting month**

| UTC time | Start orbit | Stop orbit | Mode (Asynchronous or Synchronous) | Calibration (CAL) or Dark Sky Area (DSA) |
|---|---|---|---|---|
| 02 Apr 2004 22:13:52 | 10934 | 10934 | A | DSA98 |
| 10 Apr 2004 07:57:20 | 11040 | 11047 | A | CAL60 |
| 17 Apr 2004 16:00:12 | 11145 | 11145 | A | DSA99 |
| 24 Apr 2004 15:40:05 | 11245 | 11245 | A | DSA100 |

**Table 4.1-3: Historic CTI Tables**

| CTI filename | Dissemination to FOCC |
|---|---|
| CTI_SMP_GMVIEC20030716_123904_00000000_00000004_20030715_000000_20781231_235959.N1 | 16-JUL-2003 |
| CTI_SMP_GMVIEC20021104_075734_00000000_00000003_20021002_000000_20781231_235959.N1 | 06-NOV-2003 |
| CTI_SMP_GMVIEC20021002_082339_00000000_00000002_20021002_000000_20781231_235959.N1 | 07-OCT-2003 |
| CTI_SMP_GMVIEC20020207_154455_00000000_00000000_20020301_032709_20781231_235959.N1 | 21-FEB-2002 |

## *4.2 Thermal Performance*

Since the beginning of the mission the hot pixel and RTS phenomena are producing a continuous increase of the dark charge signal within the CCD detectors (see section 4.4.1). In order to minimize this effect, three successive CCD cool down were performed in orbits 800 (25th April 2002), 1050 (13th May 2002) and 2780 (11th September 2002) with a total decrease in temperature of 14 degrees.

Fig. 4.2-1 and 4.2-2 display, respectively, the overall temperature variation and the temperature variation around the Ascending Node Crossing (ANX) time with a resolution of 0.4 degrees (coding accuracy for level 0 data). The CCD temperatures during April are 0.5 degrees higher than the ones registered in March and about one degree higher than April 2003. The expected seasonal variation of the temperatures with amplitude of around one degree can be clearly observed. It can be observed also a small overall temperature increase due to the ageing of the radiators. The peaks that occur mainly in spectrometer B1 and B2 are also to be noted. They happen a little before the ANX for some consecutive orbits and every 8-10 days. Their origin is still not known, as we did not find any correlation between these peaks and other activities carried out by other ENVISAT instruments. The CCD temperature at almost the same latitude location (fig. 4.2-2) is monitored in order to detect any inter-orbital temperature variation.

The decrease observed on 24th March 2003, twice in September 2003 and at the beginning of December 2003 in all detectors is after GOMOS switch off periods, when the instrument did not have enough time to reach the nominal temperature before starting the measurements.

The orbital temperature variation of the detector SPB2 (fig. 4.2-3 & 4.2-4) is nominal and around 2.5 degree. The stability of the temperature during the orbit is important because it affects the position of the interference patterns. The phenomenon of the interference is present mainly in SPB and this Pixel Response Non-Uniformity (PRNU) is corrected during the processing.

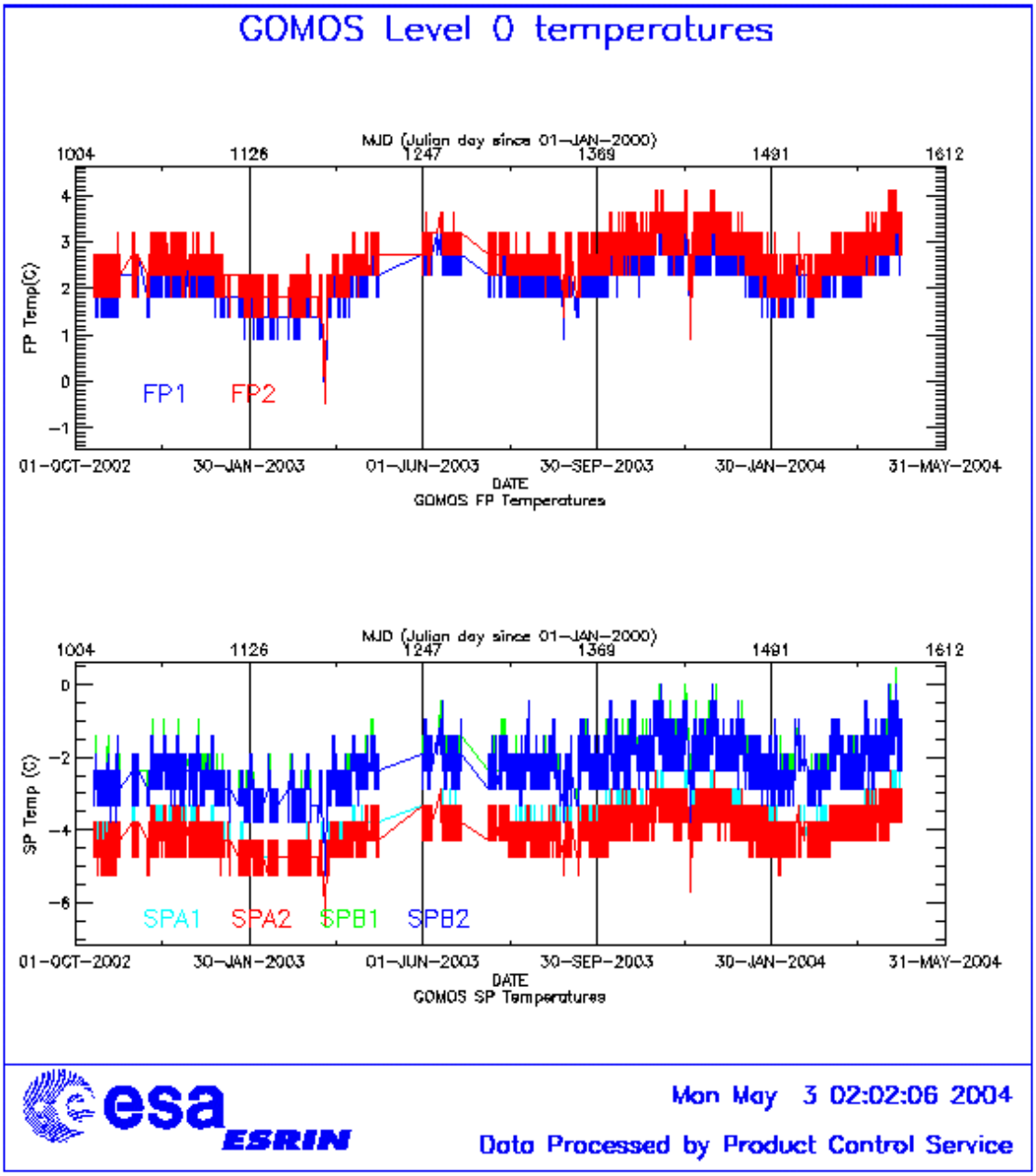


**Figure 4.2-1: Level 0 temperature evolution of all GOMOS CCD detectors since October 2002 until the end of the reporting month**

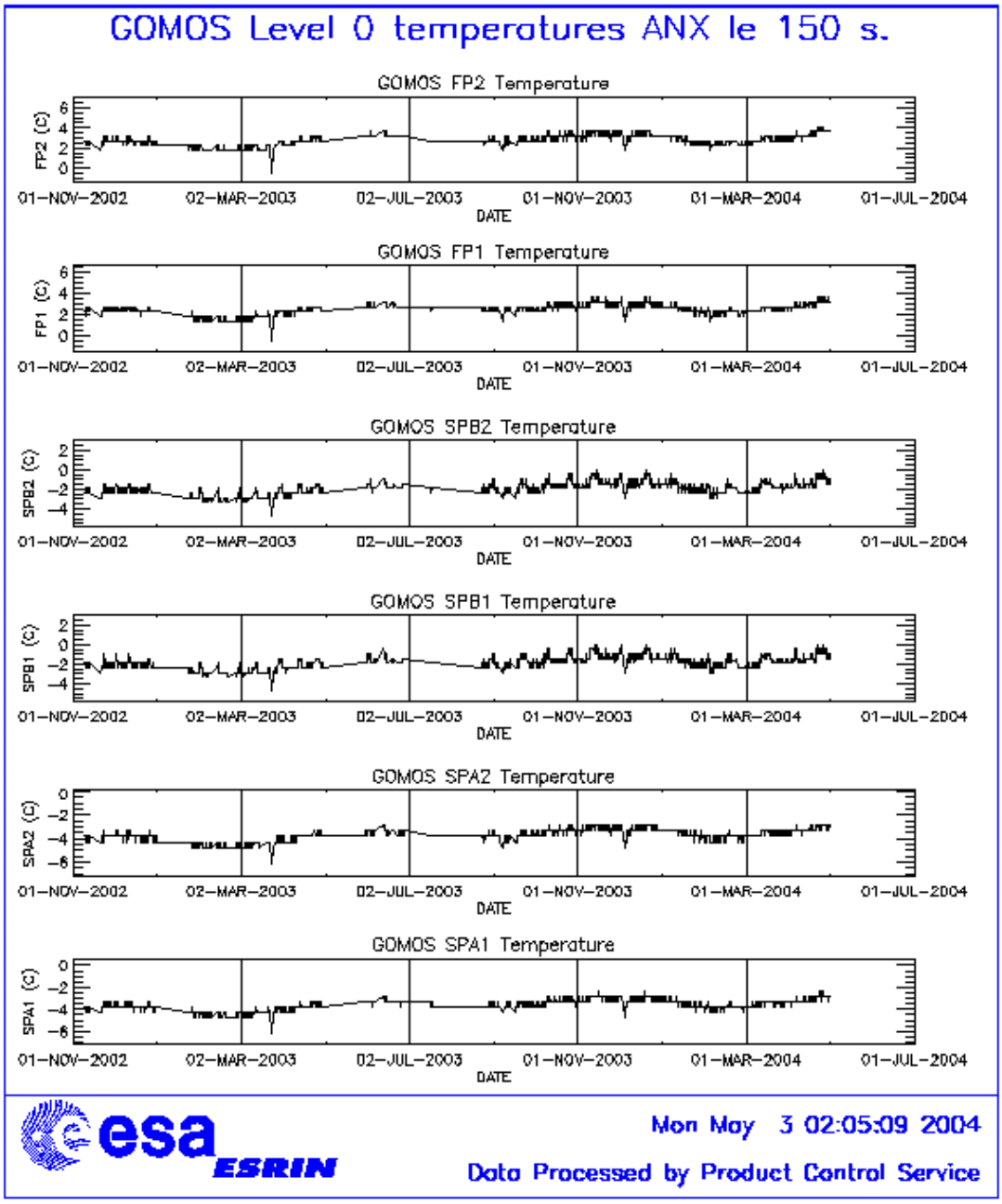


**Figure 4.2-2**: **Level 0 temperature evolution of all GOMOS CCD detectors around ANX since November 2002 until the end of the reporting month**

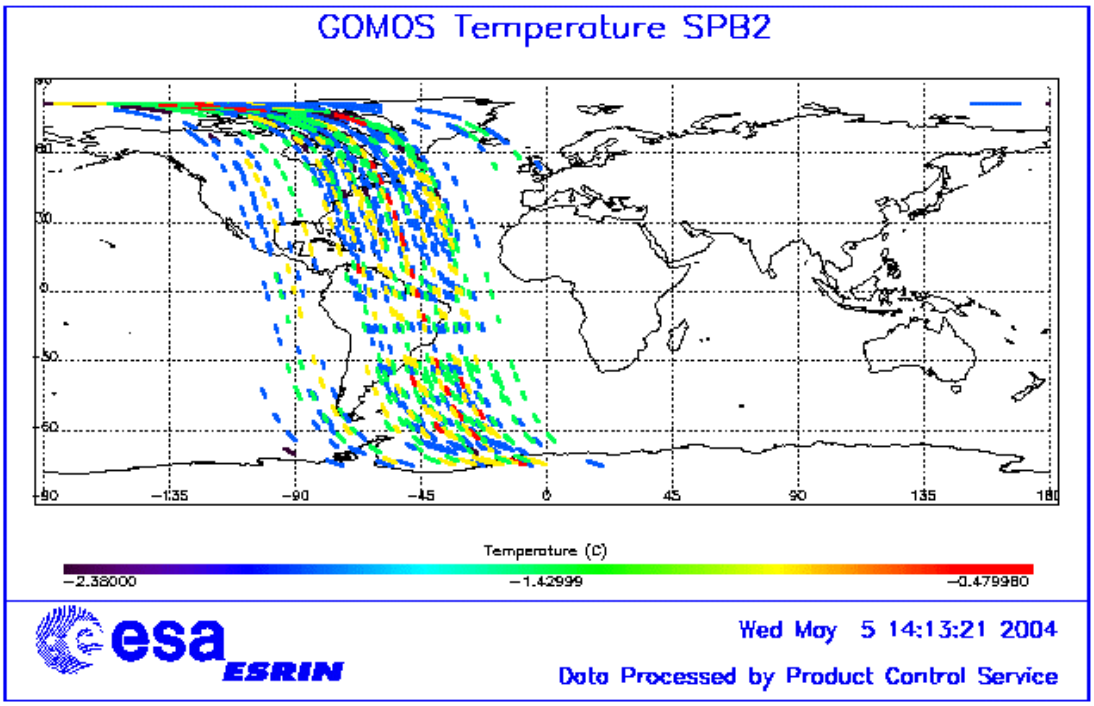


**Figure 4.2-3: Ascending orbital variation of SPB2 temperature during some orbits on April 2004**

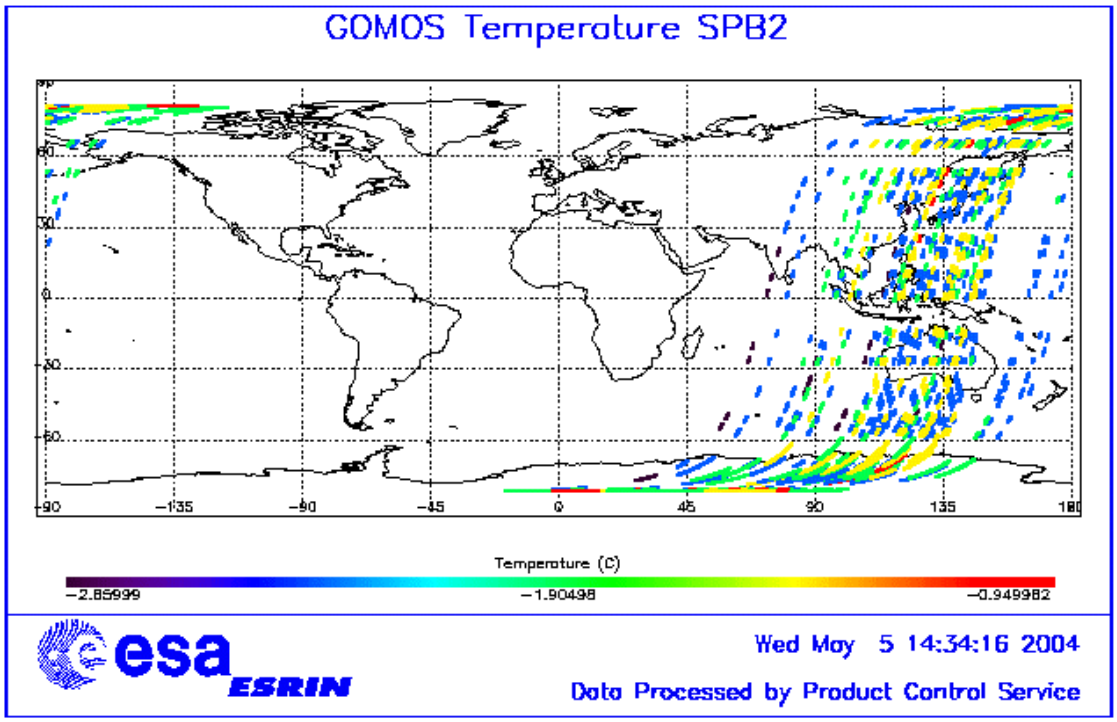


**Figure 4.2-4: Descending orbital variation of SPB2 temperature during some orbits on April 2004**

## 4.3 Optomechanical Performance

- Version GOMOS/4.00 and previous ones:

In the processors versions of GOMOS (GOMOS/4.00 and previous) the spectra is expected to be aligned along CCD lines, and therefore use only a single average line index per CCD. In table 4.3-1 the mean values of the location of the star signal for all the calibration analysis done are reported. The 'left' and 'right' values are calculated (the whole interval is not used) because the spectra present a slight slope, more pronounced in the spectrometer B (see fig. 4-3.1). In table 4.3-2, mean values of the location of the star signal are calculated for some specific wavelength intervals. These intervals have been changed between the calibration performed in September 2002 and the ones performed afterwards (until November 2003). Table 4.3-3 reports the average location of the star spot on the photometer 1 and 2 CCD.

- Version GOMOS/4.02:

In the actual processor version (GOMOS/4.02) operational since 23rd March 2004, a Look Up Table (LUT) gives the line index of the spectra location as a function of the wavelength (blue dots in fig. 4.3-1). A new calibration exercise has been performed during April. The position of the stellar spectra of star id 31, 18 and 4 observed in dark-limb spatial spread monitoring mode have been averaged above 120 km altitude and compared to the values of the LUT. The results confirm the LUT values (see table 4.3-4) so for the time being there is no need to update the LUT.

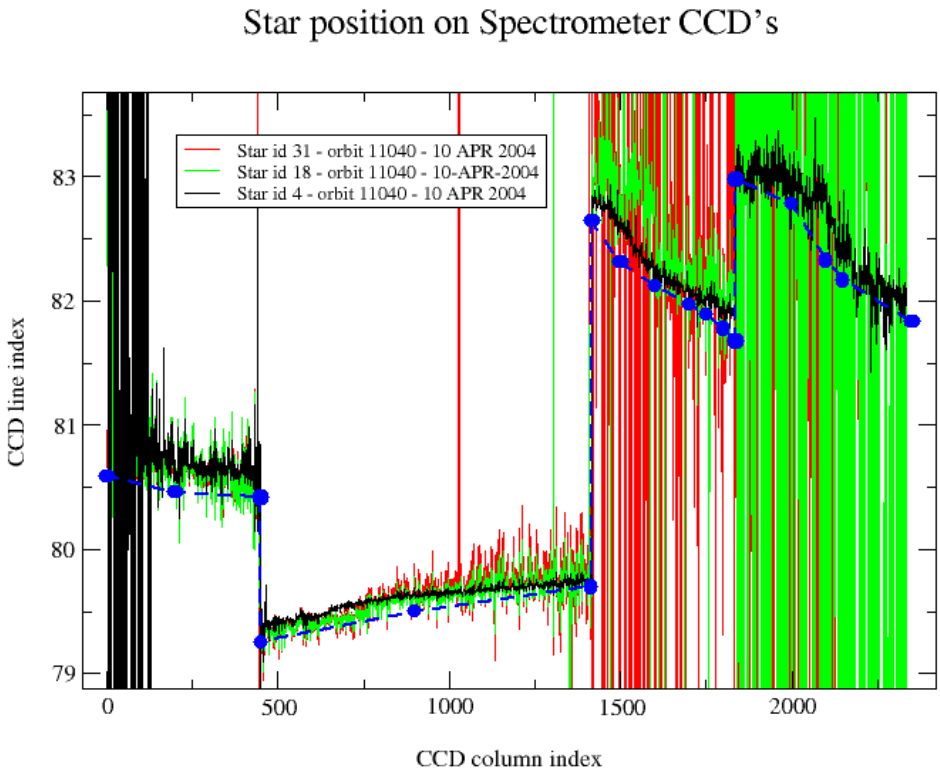


**Figure 4.3-1: Average position of star spectra on the CCD**

**Table 4.3-1: Mean value of the location of the star signal during the occultation at the edges of every band (mean over 50 values, filtering the outliers)**

| | UV (SPA1) left/right | VIS (SPA2) left/right (Inverted spectra) | IR1 (SPB1) left/right | IR2 (SPB2) left/right |
|---|---|---|---|---|
| **11/09/2002** | 80.7/80.7 | 79.8/79.5 | 82.8/81.9 | 83.1/82.1 |
| **01/01/2003** | 80.7/80.6 | 79.8/79.5 | 82.8/82.0 | 83.2/82.2 |
| **17/07/2003 & 02/08/2003** | 80.7/80.7 | 79.8/79.5 | 82.8/81.9 | 83.1/82.1 |
| **08/11/2003** | 80.7/80.6 | 79.8/79.5 | 82.8/81.9 | 83.1/82.1 |

**Table 4.3-2: Mean value of the location of the star signal during the occultation (as table 4.3-1) but now within some wavelength intervals**

| | UV (SPA1) | VIS (SPA2) | IR1 (SPB1) | IR2 (SPB2) |
|---|---|---|---|---|
| **11/09/2002 wl range (nm)** | 80.8 [300-330] | 79.8 [500-530] | 82.6 [760-765] | 82.9 [937-942] |
| **01/01/2003 wl range (nm)** | 80.6 [350-360] | 78.6 [650-670] | 81.6 [760-765] | 80.3 [935-945] |
| **02/08/2003** | 80.6 | 79.7 | 82.5 | 82.8 |
| **08/11/2003** | 80.6 | 79.9 | 82.4 | 82.8 |

**Table 4.3-3: Average column and row pixel location of the star spot on the photometer CCD during the occultation**

| | FP1 (column/row) | FP2 (column/row) |
|---|---|---|
| **11/09/2002** | 11/4 | 5/5 |
| **01/01/2003** | 10/4 | 6/4.9 |
| **02/08/2003** | 10/4 | 6/5 |
| **08/11/2003** | 10/4 | 6/5 |

**Table 4.3-4: Location of the star signal on the CCD's (corresponding to fig. 4.3-1)**

| Pixel Column | LUT (Pixel line) | Calibration on 10-APR-2004 |
|---|---|---|
| **0** | **80.59** | 80.80 |
| **20** | **80.46** | 80.60 |
| **449** | **80.42** | 80.50 |
| **450** | **79.25** | 79.39 |
| **900** | **79.50** | 79.63 |
| **1415** | **79.70** | 79.76 |
| **1416** | **82.64** | 82.80 |
| **1500** | **82.31** | 82.60 |
| **1600** | **82.12** | 82.22 |
| **1700** | **81.97** | 82.04 |
| **1750** | **81.89** | 81.98 |
| **1800** | **81.78** | 81.91 |
| **1835** | **81.68** | 81.88 |
| **1836** | **82.98** | 83.10 |
| **2000** | **82.78** | 82.90 |
| **2100** | **82.33** | 82.70 |
| **2150** | **82.17** | 82.40 |
| **2350** | **81.83** | 82.00 |

## *4.4 Electronic Performance*

### 4.4.1 DARK CHARGE EVOLUTION AND TREND

The trend of Dark Charge (DC) is of crucial importance for the final quality of the products, and is therefore subject to intense monitoring. As part of the DC there is:

- "Hot pixels", a pixel is "hot" when its dark charge exceeds its value measured on ground, at the same temperature, by a significant amount.
- RTS phenomenon (Random Telegraphic Signal), it is an abrupt change (positive or negative) of the CCD pixel signal, random in time, affecting only the DC part of the signal and not the photon generated signal.

The temperature dependence of the DC would make this parameter a good indicator of the DC behaviour, but the hot pixels and the RTS are producing a continuous increase of the DC (see trend in fig. 4.4-1 and 4.4-2). To take into account these phenomena, since version GOMOS/4.00 (actual one is GOMOS/4.02) a DC map per orbit is extracted from a Dark Sky Area (DSA) observation performed around ANX (full dark conditions). For every level 1b product (occultation), the actual thermistor temperature of the CCD is used to convert the DC map measured around ANX into an estimate of the DC at the time (and different temperature) of the actual occultation. When the DSA observation is not available, the DC map inside the calibration product that was measured at a given thermistor reference temperature is used; again, the actual thermistor temperature of the CCD is used to compute the actual map. Table 4.4-1 reports the list of products that used the DC maps inside the calibration file due to the non-availability of

DSA observation. A “CAL DC map with no T dep.” means that, as the temperature information was not available for the occultation, the DC map used is exactly the one inside the Calibration product.

**Table 4.4-1: Table of level 1b products that used the Calibration DC maps instead of the DSA observation**

| Product Name | DC Information |
|---|---|
| GOM_TRA_1PNPDE20040406_032425_000000612025_00405_10980_0000.N1 | DC map with no T dep. (12) |
| GOM_TRA_1PNPDE20040406_032609_000000692025_00405_10980_0001.N1 | DC map used (0) |
| GOM_TRA_1PNPDE20040406_032839_000000722025_00405_10980_0002.N1 | DC map used (0) |
| GOM_TRA_1PNPDE20040406_033047_000000432025_00405_10980_0003.N1 | DC map used (0) |
| GOM_TRA_1PNPDE20040406_033321_000000552025_00405_10980_0004.N1 | DC map used (0) |
| GOM_TRA_1PNPDE20040406_033519_000000452025_00405_10980_0005.N1 | DC map used (0) |
| GOM_TRA_1PNPDE20040406_033649_000000462025_00405_10980_0006.N1 | DC map used (0) |
| GOM_TRA_1PNPDE20040406_033849_000000432025_00405_10980_0007.N1 | DC map used (0) |
| GOM_TRA_1PNPDE20040406_034029_000000522025_00405_10980_0008.N1 | DC map used (0) |
| GOM_TRA_1PNPDE20040406_034331_000001322025_00405_10980_0009.N1 | DC map used (0) |
| GOM_TRA_1PNPDE20040427_022337_000000442026_00204_11280_0000.N1 | DC map with no T dep. (12) |
| GOM_TRA_1PNPDE20040427_022836_000000742026_00204_11280_0001.N1 | DC map used (0) |
| GOM_TRA_1PNPDE20040427_023112_000000462026_00204_11280_0002.N1 | DC map used (0) |
| GOM_TRA_1PNPDE20040427_023249_000000562026_00204_11280_0003.N1 | DC map used (0) |
| GOM_TRA_1PNPDE20040427_023447_000000532026_00204_11280_0004.N1 | DC map used (0) |
| GOM_TRA_1PNPDE20040427_023629_000000412026_00204_11280_0005.N1 | DC map used (0) |
| GOM_TRA_1PNPDE20040427_023928_000000412026_00204_11280_0006.N1 | DC map used (0) |
| GOM_TRA_1PNPDE20040427_024147_000000772026_00204_11280_0007.N1 | DC map used (0) |

In fig. 4.4-1 and 4.4-2 it is plotted the average DC inserted by the processor into the level 1b data products for the spectrometers SPA1 and SPB2 (per band: upper, central and lower). From the figures, it can be noted that there is an increase of DC for the last month as expected.

The same DC values are plotted in fig. 4.4-3 but for some occultations belonging only to the reporting month.

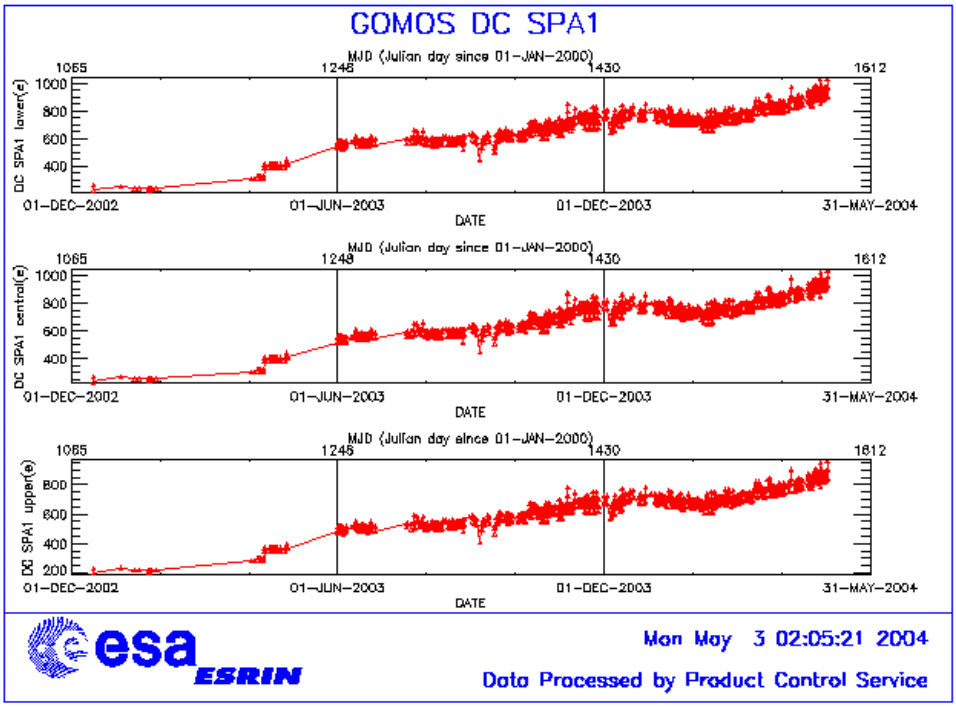


**Figure 4.4-1: Mean DC evolution on SPA1 since 15th December 2002 until the end of the reporting month**

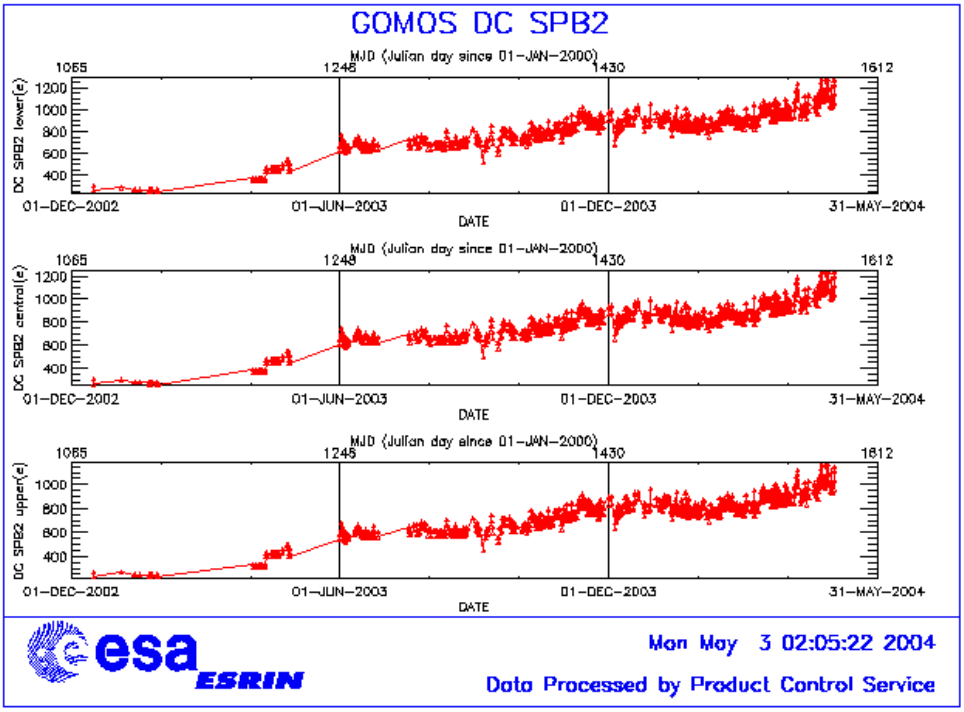


**Figure 4.4-2: Mean DC evolution on SPB2 from 15th December 2002 until the end of the reporting month**

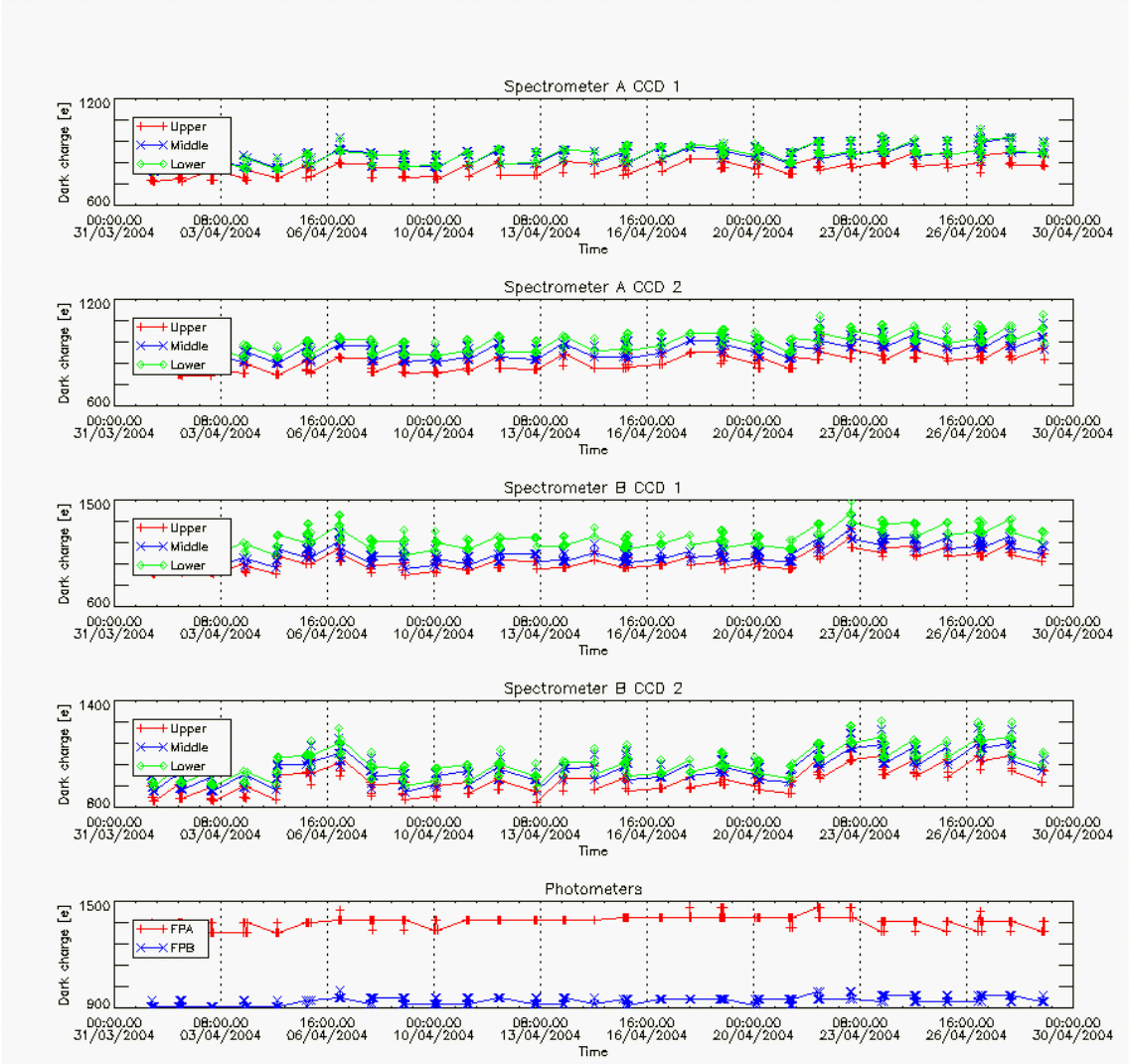


**Figure 4.4-3: Mean Dark Charge of spectrometers and photometers during reporting month.**

## 4.4.2 SIGNAL MODULATION

A parasitic signal was found to be systematically present, added to the useful signal, at least for spectrometers A1 and A2. The modulation is corrected in the data processing, but the modulation signal standard deviation is routinely monitored in order to detect any trend (fig. 4.4-4).

The modulation standard deviation, for every spectrometer, is characterised as follows:

$$\sigma_{mod} = (\text{'static noises'} - \text{'total static variance'})^{1/2} / \text{gain} \qquad \text{(in ADU)}$$

- The 'static noises' are calculated from the DSA observation performed once per orbit
- The 'total static variance' is obtained from ADF data (electronic chain noise, quantization noise).

The standard deviation of the modulation signal (fig. 4.4-4) presents high values after the inclusion at the end of March of the ESRIN level 0 data. Although it is to be confirmed, it is suspected that the South Atlantic Anomaly is the cause of these unexpected peaks. The quality of ESRIN data, in particular over the SAA zone, is thus under investigation.

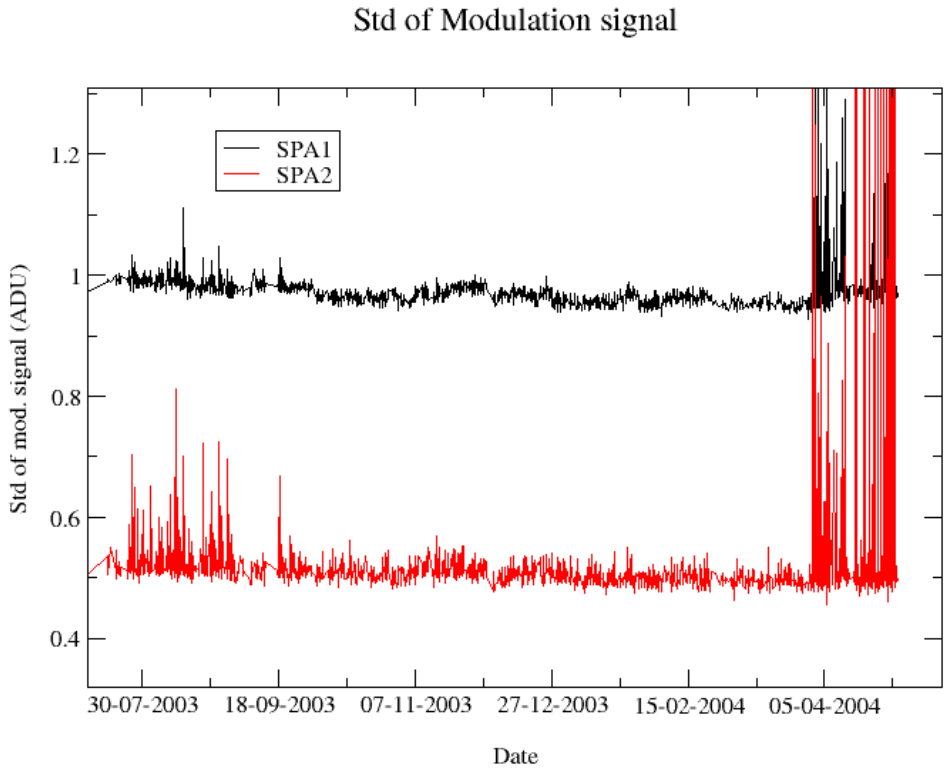


**Figure 4.4-4: Standard deviation of the modulation signal**

## 4.4.3 ELECTRONIC CHAIN GAIN AND OFFSET

No new electronic chain gain and offset calibration has been done during the reporting month so these results have been already presented in previous MR.

The routine monitoring of the ADC offset is a good indicator of the ageing of the instrument electronics. During the definition of this routine activity, an exercise has been done to analyze the variation of the ADC offset using the calibration observation in linearity mode (orbits 2810, 4384, 4834, 5219 and 5734). The fig. 4.4-5 presents the evolution of the calibrated ADC offset for each spectrometer electronic chain. The unexpected increase of this offset seems to be due to an external contribution. In the ADC offset calibration procedure, linearity observations are used with two integration times of 0.25 and 0.50 seconds to extrapolate to an integration time of 0 seconds that give the complete chain offset and not only the ADC offset. The complete offset contains any possible offsets, and especially the static dark charge (i.e. the dark charge that does not depend of the spectrometer integration time). If the memory area of the CCD is affected by the generation of hot pixels (this is confirmed by the presence of vertical lines visible

in the measurement maps in spatial spread monitoring mode), it becomes that the increase observed in fig. 4.4-5 is due to these new hot pixels.

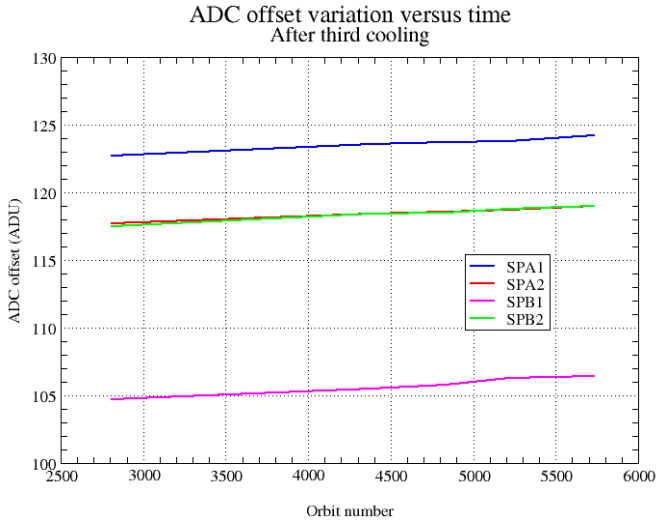


**Figure 4.4-5: Evolution of the ADC offset for each spectrometer electronic chain**

Next task consists in completing the analysis to confirm that the offset increase is due to the hot pixels in memory area. This can be proven by the study of the noise due to the increased dark charge. The increase of ADC offset will be assumed to be equal to the increase of 'static dark charge' and the corresponding noise will be computed and compared to the increase of the signal variance residual.

If we keep the ADC offset constant, as it is also used to compute the dark charge at band level used to correct the samples in the level 1b processing, the increase of the static dark charge - not taken into account in the ADC offset - is compensated by an artificial increase of the calibrated dark charge. So, the star and limb spectra are correctly corrected for dark charge. A small bias can be added to the instrument noise due to the incorrect dark charge level. Anyway, this quantity is not large enough to require a modification of the ADC offset value.

## *4.5 Acquisition, Detection and Pointing Performance*

### 4.5.1 SATU NOISE EQUIVALENT ANGLE

The Star Acquisition and Tracking Unit (SATU) noise equivalent angle (SATU NEA) consists of the statistical angular variation of the SATU data above the atmosphere.
The mean of the standard deviation (std over the 50 values per measurement) above 105 km are computed for every occultation, giving two values per occultation: one in the 'X' direction, one in the 'Y' direction. A mean value per day in every direction and limb is calculated and monitored in order to assess instrument performance in terms of star pointing. The thresholds are 2 and 3 micro radians in 'X' and 'Y' directions respectively. Before May 2003, data above 90 km have been considered (instead of 105 km) but from May 2003 on, data taken in the mesospheric oxygen layer (located around 100 km altitude) have

been avoided because they could cause fluctuations on the SATU data. Also the products with errors (error flag set) are discarded from May 2003 onwards.

It can be seen in fig. 4-5.1 that the SATU NEA are well below the thresholds, there was even a slight decrease mainly for the Y-axis in bright limb during the reporting month. The results for some occultations belonging to previous months (monthly averages) are presented in fig. 4.5-2, where no trend is visible so far.

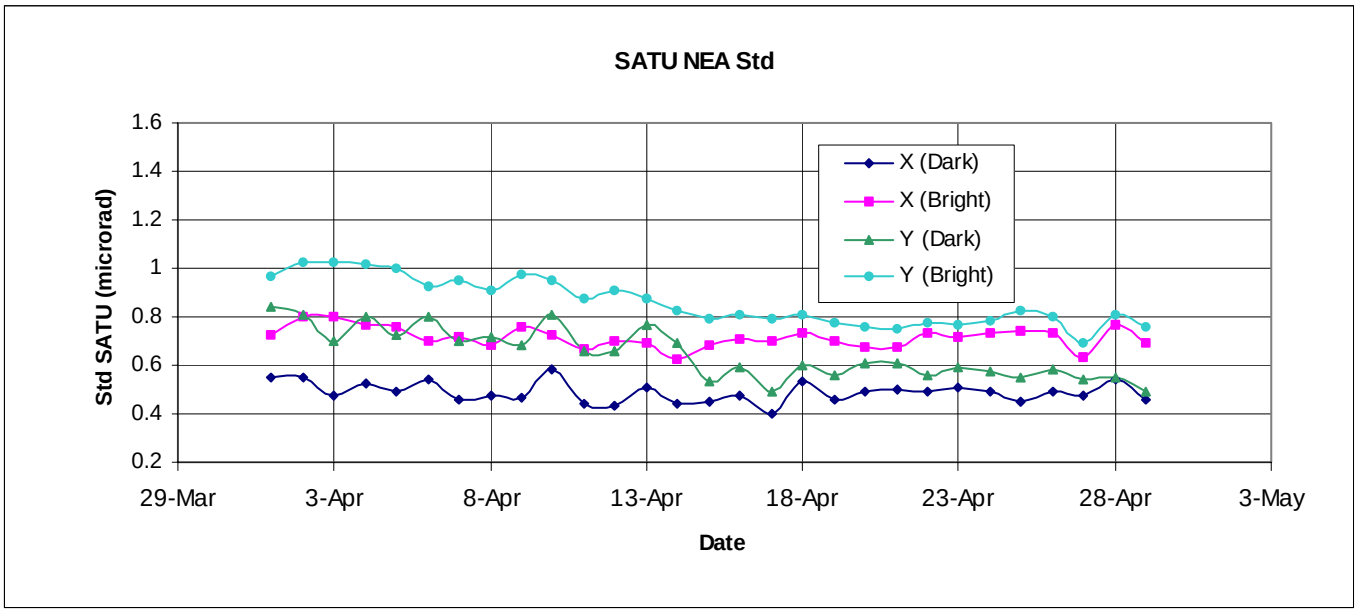


**Figure 4.5-1: Average value per day of SATU NEA std above 105 km**

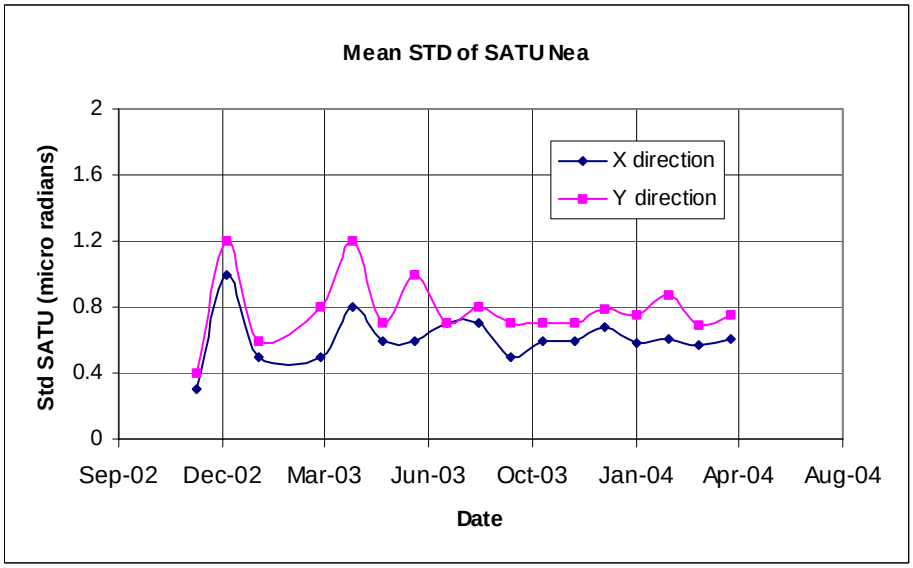


**Figure 4.5-2: Average value per month of SATU NEA std above 105 km**

## 4.5.2 TRACKING LOSS INFORMATION

This verification consists of the monitoring of the tangent altitude at which the star is lost. It is an indicator of the pointing performance although it is to be considered that star tracking is also lost due to the presence of clouds and hence not only due to deficiencies in the pointing performance. Therefore, only the detection of any systematic long-term trend is the main purpose of this monitoring. The recent results are presented in fig. 4.5-3 and fig. 4.5-4:

- The dependence of the altitude at which tracking is lost on the magnitude of the star is very small because the tracking is mainly lost due to the refraction and the scintillation that depend on the atmospheric conditions.
- There are two stars lost at high altitude in dark limb (fig. 4.5-3). They correspond to the star id 163 (1st April) and 100 (13th April). They are partial occultations (at the beginning or at the end of the orbit). The entire occultations are included within the previous of the following orbit.
- In fig. 4.5-4 there is one star lost at high tangent altitude. It is the star id number 5 on 4th April.
- Some statistics are given in fig. 4.5-5 calculated for a set of data and not for the whole months. For the moment, no trend is visible in the plot.

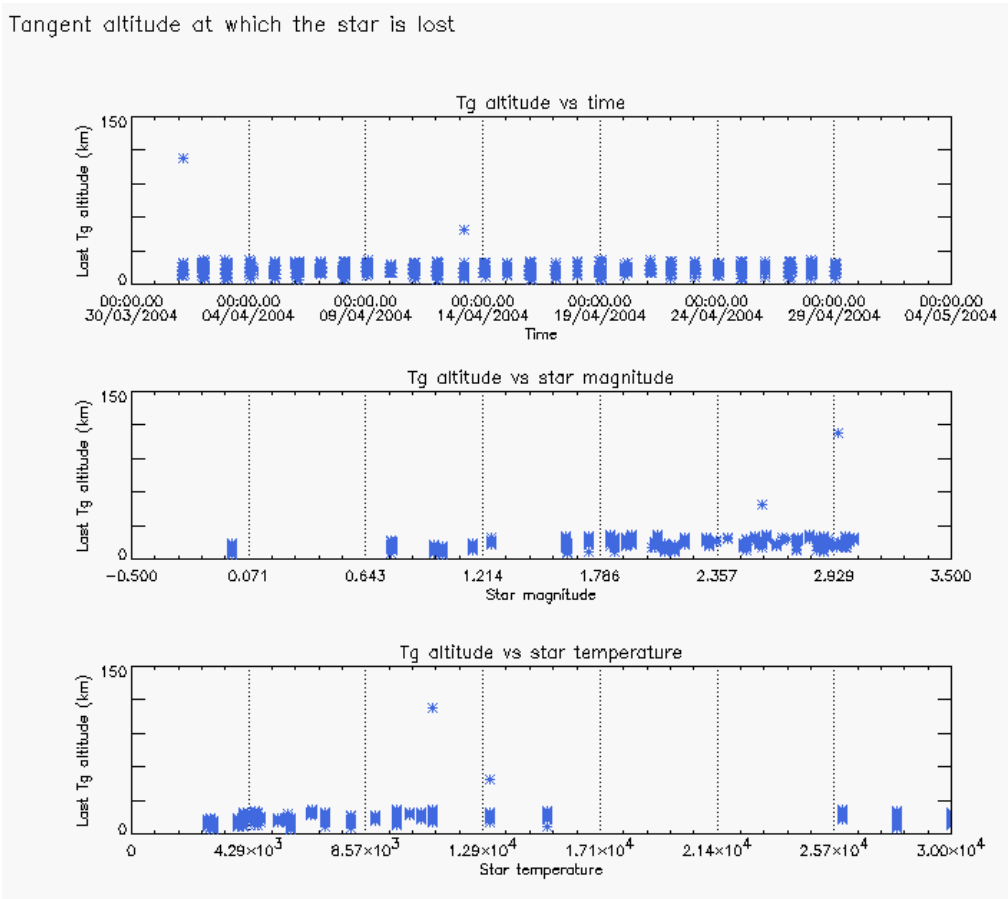


**Figure 4.5-3: Last tangent altitude of the occultation (dark limb), point at which the star is lost**

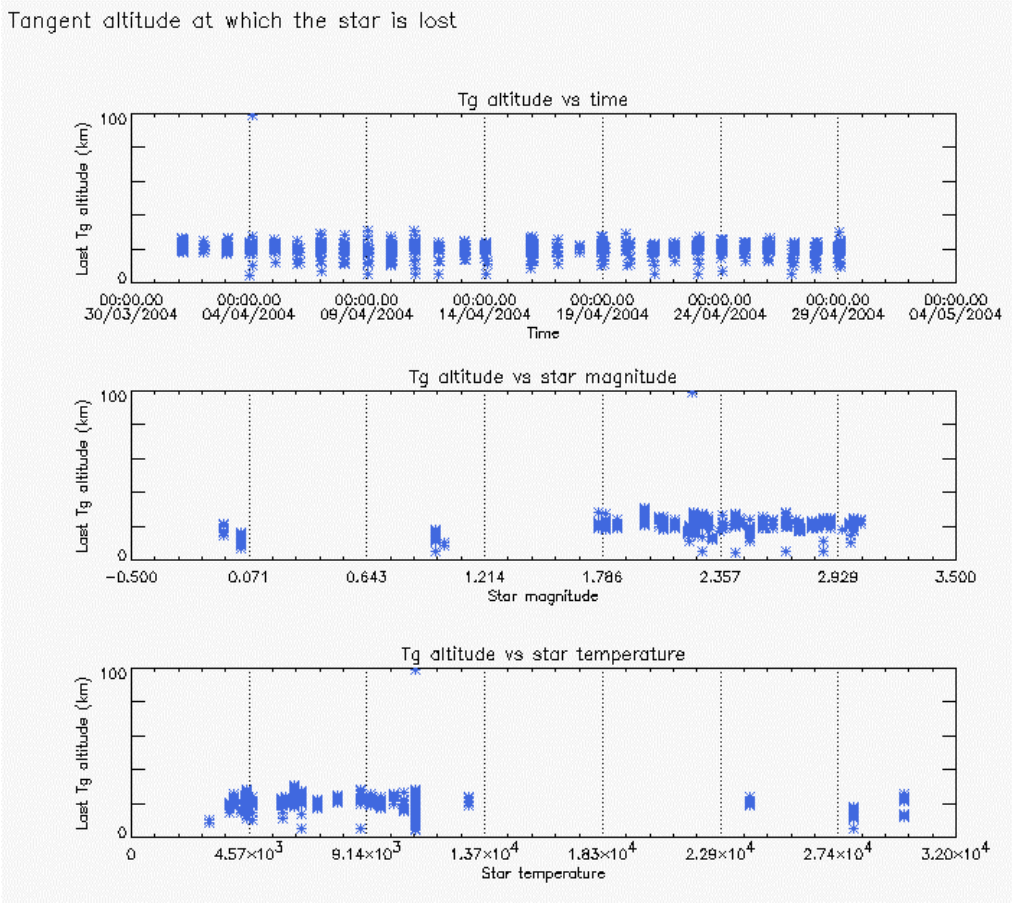


**Figure 4.5-4: Last tangent altitude of the occultation (bright limb), point at which the star is lost**

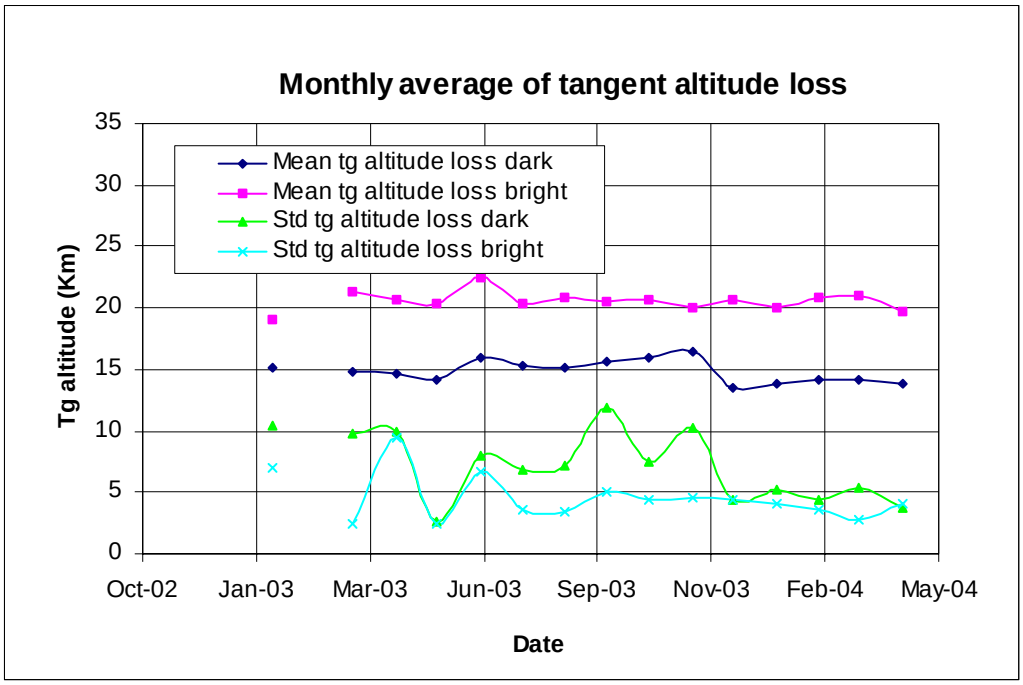


**Figure 4.5-5: Monthly mean tangent altitude (and Std) at which the star is lost since January 2003**

## 4.5.3 MOST ILLUMINATED PIXEL (MIP)

The MIP (Most Illuminated Pixel) is the star position on the SATU CCD in detection mode and it is recorded in the housekeeping data. The nominal centre of the SATU is pixel number **145** in elevation and number **205** in azimuth. The detection of the stars should not be far from this centre. As can be seen in fig. 4.5-6 the azimuth is always well within the threshold (table 4.5-1) since September 2002 even if a small variation is present. The elevation MIP has a significant variation (see the *note* below) till 12th December 2003 when a new PSO algorithm was activated in order to reduce the deviations of the ENVISAT platform attitude with respect to the nominal one. The annual amplitude of the MIP displacement is decreased from 18-20 pixels to 8-10 that means an important improvement of the ENVISAT pointing performance. This result confirms that, until now, the algorithm is working as expected. Anyway, the MIP displacement will continue to be carefully monitored during the following months. Fig. 4.5-7 shows the standard deviation of azimuth and elevation that should be within the thresholds of table 4.5-1. The peaks observed mean that one (or more) star/s where detected very far from the SATU centre and, in this case, the star/s is lost during the centering phase (see section 3.2 for stars lost in centering).

*Note*: A MIP variation onto the SATU CCD of 50 pixels corresponds to a de-pointing of 0.1 degrees

**Table 4.5-1: MIP Thresholds**

| | | |
|---|---|---|
| **MIP X** | **Mean delta Az** | [198 - 210] |
| | **Std delta Az** | 7 |
| **MIP Y** | **Mean delta El** | [145 – 154] |
| | **Std delta El** | 4 |

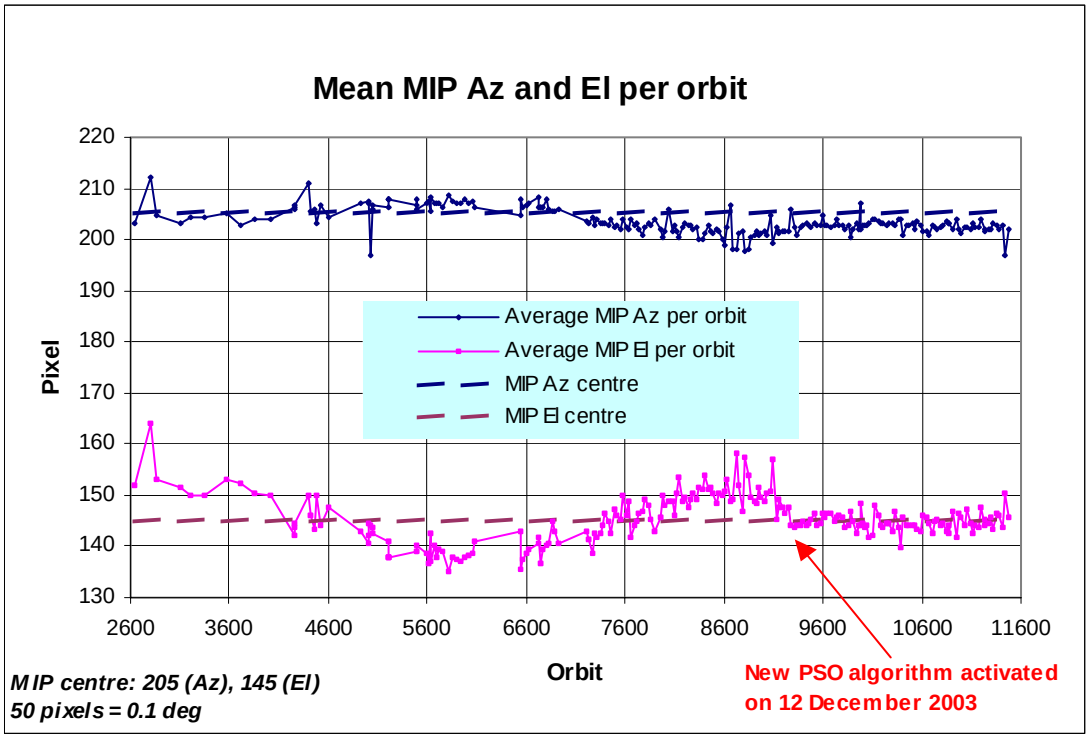


**Figure 4.5-6: Mean values of MIP for some orbits since 1st September 2002 (see table 4.5-1)**

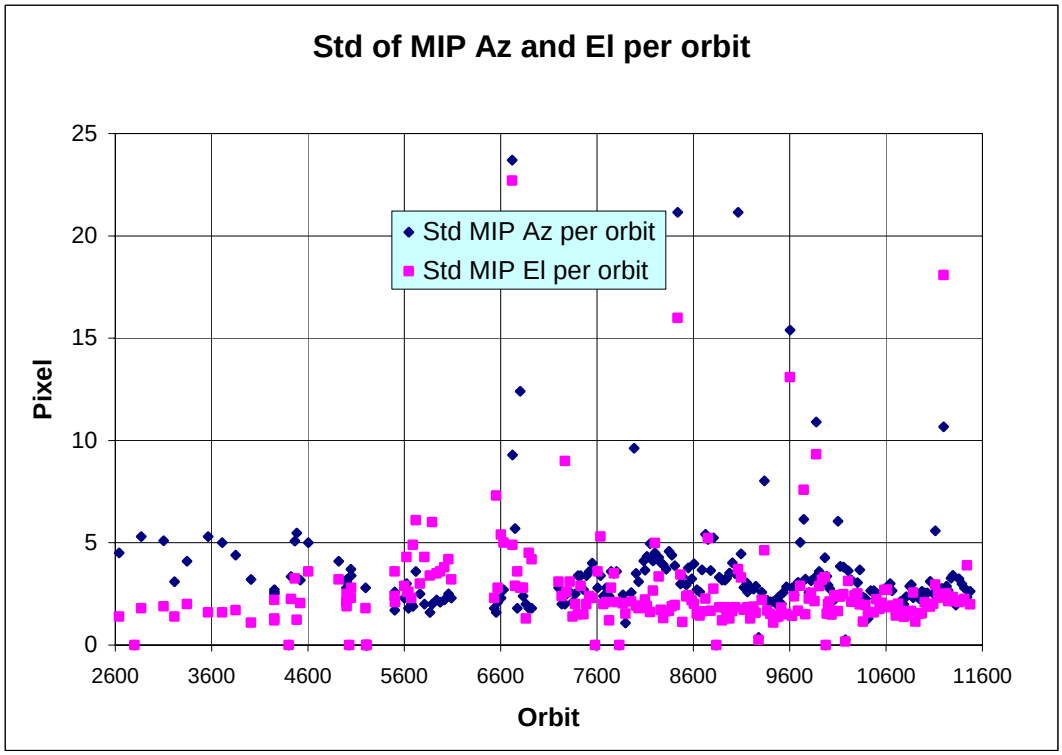


**Figure 4.5-7: Standard deviation of MIP Azimuth and Elevation for some orbits since 1st September 2002 until end of reporting period (see table 4.5-1)**

# 5 LEVEL 1 PRODUCT QUALITY MONITORING

## *5.1 Processor Configuration*

### 5.1.1 VERSION

About 10% of GOM_TRA_1P products have been received in the PCF for routine quality control and long term trend quality monitoring. The current level 1-processor software version for the operational ground segment is GOMOS/4.02 (see table 5.1-1). The product specification is PO-RS-MDA-GS2009_10_3H. This processor has been cleared for initial level 1 data release, with a disclaimer for known artefacts that are currently being resolved and will be implemented in the next release (http://envisat.esa.int/dataproducts/availability).

Cal/Val teams are supplied with selected data sets generated by the prototype processor GOPR 6.0a. See table 5.1-2 for prototype level 1b versions and modifications.

**Table 5.1-1: PDS level 1b product version and main modifications implemented**

| Date | Version | Description of changes |
|---|---|---|
| 23-MAR-2004 | Level 1b version 4.02 at PDHS-E and PDHS-K | Algorithm baseline level 1b DPM 6.0<br>• Adding a new calibration parameters (these values are hard coded at the moment)<br>• Removal of redundancy chain from code<br>• Modifications in the processing to apply new configuration and calibration parameter<br>• New algorithm to determine between dark, twilight and bright limb and to handle data accordingly<br>• Added handling of source packages with invalid packet header<br>• Added enumerations for all configuration flags<br>• See ref. [2] for more details |
| 31-MAY-2003 | Level 1b version 4.00 at PDHS-E and PDHS-K | Algorithm baseline level 1b DPM 5.4:<br>• Modulation correction step added after the cosmic rays detection processing<br>• Inversion of the non-linearity and offset corrections<br>• Modification of the computation of the estimated background signal measured by the photometers: use the spectrometer radiometric sensitivity curve and the photometer transfer function.<br>• Use of the dark charge map at orbit level computed from the DSA (dark sky area) if any in the level 0 product<br>• Implementation of a new unfolding algorithm for the photometer samples<br>• See ref. [2] for more details |
| 21-NOV-2002 | Level 1b version 3.61 at PDHS-E and PDHS-K | Algorithm baseline DPM 5.3:<br>• Review of some default values<br>• New definition of one PCD flag (atmosphere)<br>• Temporal interpolation of ECMWF data<br>• See ref. [2] for more details |

**Table 5.1-2: GOPR level 1b product version and main modifications implemented**

| Date | Version | Description of changes |
|---|---|---|
| 17-MAR-2004 | GOPR 6.0a | • Provide SFA and SATU angles in degrees<br>• Elevation angle dependency of the reflectivity LUT added in the algorithms<br>• Ratio upper/star signal added (FLAGUC)<br>• Add Dark Charge used for dark charge correction (per band)<br>• Flag for illumination condition (PCDillum)<br>• Minimum sample value for which the cosmic rays detection processing is applied (Crmin) is a function of gain index<br>• Logic for computation of the flags attached to the reference star spectrum (Flref) modified<br>• Add the computation of the sun direction in the inertial geocentric frame to be written in the level 1b and limb products.<br>• Spectrometer effective sampling time added<br>(To be completed) |

| | | |
|---|---|---|
| 25-JUL-2003 | GOPR 5.4f | • The demodulation process is applied only in full dark limb and twilight limb conditions. |
| 17-JUL-2003 | GOPR 5.4e | • Sun zenith angle is computed in the geolocation process. The occultation is now classified into (0) full dark limb condition, (1) bright limb condition and (2) twilight limb condition.<br>• No background correction applied in full dark limb condition. The location of the image of the star spectrum on the CCD array is no more aligned with the CCD lines. |
| 02-JUL2003 | GOPR 5.4d | • The maximum number of measurements is set to 509 (instead of 510) in the GOPR prototype. |
| 17-MAR-2003 | GOPR 5.4c | • Modification of the CAL ADFs (update of the limb radiometric LUT). The products are affected only if the limb spectra are converted into physical units<br>• Modifications to allow compatibility with ACRI computational cluster (no modifications of the results)<br>• Modification of the logic to handle dark charge map refresh at orbit level (DSA data is now directly processed by the level 1b processor if available in the level 0 product). No impact on the results |
| 21-FEB-2003 | GOPR 5.4b | • DC map values are rounded when written in the level 1b product<br>• Modification of the CAL ADFs (update of the wavelength assignment of SPB1 and SPB2)<br>• Modify the computation of flag_mod in the modulation correction routine |
| 17-JAN-2003 | GOPR 5.4a | • use the start and stop dates of the occultation when calling the CFI interpol instead of start and stop dates of the level 0 product<br>• modify the ECMWF filename information in the SPH of the level 1b and limb products |

## 5.1.2 AUXILIARY DATA FILES (ADF)

The ADF's files in tables 5.1-3, 5.1-4, 5.1-5, 5.1-6 and 5.1-7 have been disseminated to the PDS during the whole mission. For every type of file, the validity runs from the start validity time until the start validity time of the following one, but if an ADF file has been disseminated after the start validity time, it is obvious that it will be used by the PDS only after the dissemination time (this happens the majority of the times). As the other ADF's, the calibration auxiliary file (GOM_CAL_AX) has been updated several times in the past (table 5.1-7) but the difference is that now it is updated in a weekly basis with only new DC maps, and that is why the files used in April are reported in a separate table (table 5.1-8) that will changed from month to month. On 5$^{th}$, 13$^{th}$ and 22$^{nd}$ April new calibration ADF's were disseminated with updated DC maps of orbits 10974, 11085 and 11215 respectively (table 5.1-8). This month, also the processing level 1b configuration file (GOM_PR1_AX) has been updated (table 5.1-3). Note that the files outlined in yellow are the set of auxiliary files used during the reporting month.

**Table 5.1-3: Table of historic GOM_PR1_AX files used by PDS for level 1b products generation**

| Used by PDS for Level 1b products generation in period | GOM_PR1_AX (GOMOS processing level 1b configuration file) |
|---|---|
| 01-MAR-2002 → 29-MAR-2002 | GOM_PR1_AXVIEC20020121_165314_20020101_000000_20200101_000000<br>• Pre-launch configuration |
| 30-MAR-2002 → 14-NOV-2002 | GOM_PR1_AXVIEC20020329_115921_20020324_200000_20100101_000000<br>• Changed num_grid_upper, thr_conv and max_iter in the atmospheric GADS |

| | |
|---|---|
| Not used | GOM_PR1_AXVIEC20020729_083756_20020301_000000_20100101_000000<br>• Cosmic Ray mode + threshold<br>• DC correction based on maps<br>• Non-linearity correction disabled |
| Not used | GOM_PR1_AXVIEC20021112_170331_20020301_000000_20100101_000000<br>• Central background estimation by linear interpolation + associated thresholds |
| 15-NOV-2002 → 26-MAR-2003 | GOM_PR1_AXVIEC20021114_153119_20020324_000000_20100101_000000<br>• Same content as GOM_PR1_AXVIEC20021112_170331_20020301_000000_20100101_000000 but validity start updated so as to supersede according to the PDS file selection rules GOM_PR1_AXVIEC20020329_115921_20020324_200000_20100101_000000 |
| 27-MAR-2003 | GOM_PR1_AXVIEC20030326_085805_20020324_200000_20100101_000000<br>• Same content as GOM_PR1_AXVIEC20021112_170331_20020301_000000_20100101_000000 but validity start updated so as to supersede according to the PDS file selection rules GOM_PR1_AXVIEC20020329_115921_20020324_200000_20100101_000000 |
| 20-MAR-2004 | GOM_PR1_AXVIEC20040319_134932_20020324_200000_20100101_000000<br>• Ray tracing parameter changed: convergence criteria set to 0.1 microrad |
| 23-MAR-2004<br>*Notes*:<br>• This file was constructed from GOM_PR1_AXVIEC20030326_085805_20020324_200000_20100101_000000 (so without the ray tracing parameter changed)<br>• This file was used by the GOMOS/4.02 processors before the IECF dissemination. The dissemination was done on 25th March 2004 | GOM_PR1_AXVIEC20040316_144850_20020324_200000_20100101_000000<br>GOM_PR1 ADF for version GOMOS/4.02, changes:<br>• The central band estimation mode<br>• Atmosphere thickness<br>• Altitude discretisation |
| 02-APR-2004 | GOM_PR1_AXVIEC20040401_083133_20020324_200000_20100101_000000<br>• Ray tracing parameter changed: convergence criteria set to 0.1 microrad |

**Table 5.1-4: Table of historic GOM_INS_AX files used by PDS for level 1b products generation**

| Used by PDS for Level 1b products generation in period | GOM_INS_AX (GOMOS instrument characteristics file) |
|---|---|
| 01-MAR-2002 → 29-JUL-2002 | GOM_INS_AXVIEC20020121_165107_20020101_000000_20200101_000000<br>• Pre-launch configuration |
| 30-JUL-2002 → 12-NOV-2002 | GOM_INS_AXVIEC20020729_083625_20020301_000000_20100101_000000<br>• Factors for the conversion of the SFA angles from SFM axes to GOMOS axes |
| 13-NOV-2002 → 16-JUL-2003 | GOM_INS_AXVIEC20021112_170146_20020301_000000_20100101_000000<br>• No more invalid spectral range |

| | |
|---|---|
| Not used | GOM_INS_AXVIEC20030716_080112_20030711_120000_20100101_000000<br>• New value for SFM elevation zero offset for redundant chain: 10004 |
| 17-JUL-2003 | GOM_INS_AXVIEC20030716_105425_20030716_120000_20100101_000000<br>• Bias induct azimuth redundant value set to -0.0084 rad (-0.4813 deg) |

**Table 5.1-5: Table of historic GOM_CAT_AX files used by PDS for level 1b products generation**

| Used by PDS for Level 1b products generation in period | GOM_CAT_AX (GOMOS Stat Catalogue file) |
|---|---|
| 01-MAR-2002 | GOM_CAT_AXVIEC20020121_161009_20020101_000000_20200101_000000<br>• Pre-launch configuration |

**Table 5.1-6: Table of historic GOM_STS_AX files used by PDS for level 1b products generation**

| Used by PDS for Level 1b products generation in period | GOM_STS_AX (GOMOS Star Spectra file) |
|---|---|
| 01-MAR-2002 | GOM_STS_AXVIEC20020121_165822_20020101_000000_20200101_000000<br>• Pre-launch configuration |

**Table 5.1-7: Table of historic GOM_CAL_AX files used by PDS for level 1b products generation**

| Used by PDS for Level 1b products generation in period | GOM_CAL_AX (GOMOS Calibration file) |
|---|---|
| 01-MAR-2002 → 29-JUL-2002 | GOM_CAL_AXVIEC20020121_164808_20020101_000000_20200101_000000<br>• Pre-launch configuration |
| Not used | GOM_CAL_AXVIEC20020121_142519_20020101_000000_20200101_000000<br>• Pre-launch configuration |
| 30-JUL-2002 → 12-NOV-2002 | GOM_CAL_AXVIEC20020729_082426_20020717_193500_20100101_000000<br>• Band setting information<br>• Wavelength assignment<br>• Spectral dispersion LUT<br>• ADC offset for Spectrometers<br>• PRNU maps<br>• Thermistor coding LUT<br>• DC maps |
| Not used | GOM_CAL_AXVIEC20021112_165603_20020914_000000_20100101_000000<br>• Band setting information<br>• DC maps<br>• PRNU maps<br>• Wavelength assignment<br>• Spectral dispersion LUT<br>• Radiometric sensitivity LUT (star and limb)<br>• SP-FP intercalibration LUT<br>• Vignetting LUT<br>• Reflectivity LUT<br>• ADC offset |
| 13-NOV-2002 → 30-JAN-2003 | GOM_CAL_AXVIEC20021112_165948_20021019_000000_20100101_000000 |

| | |
|---|---|
| | • Only DC maps updated |
| 31-JAN-2003 → 11-APR-2003 | GOM_CAL_AXVIEC20030130_133032_20030101_000000_20100101_000000<br>• Only DC maps updated (using DSA of orbit 04541) |
| 12-APR-2003 → 02-JUN-2003 | GOM_CAL_AXVIEC20030411_065739_20030407_000000_20100101_000000<br>• Modification of the radiometric sensitivity curve for the limb spectra. Note that the modification of this LUT has no impact on the GOMOS processing. The LUT is just copied into the level 1b limb product for user conversion purpose.<br>• Updated DC map only (using DSA of orbit 05762). |
| 03-JUN-2003: from this date onwards, mainly updates to DC maps are done. Every month, the table of new GOM_CAL files with only DC maps updated is provided (table 5.1-8). Eventual changes do this file not corresponding only to DC maps updates will be reported in this table. | GOM_CAL_AXVIEC20030602_094748_20030531_000000_20100101_000000<br>• Updated DC maps only (using DSA of orbit 06530) |
| 13-FEB-2004 → 23-FEB-2004 | GOM_CAL_AXVIEC20040212_103916_20040209_000000_20100101_000000<br>• Update of the reflectivity LUT<br>• Updated DC maps (Orbit 10194, date 11-FEB-2004) |

**Table 5.1-8: Calibration ADF for April 2004. These files are updated (only with DC maps) in a 8-10 days basis**

| Used by PDS for Level 1b products generation in period | GOM_CAL_AX (GOMOS Calibration file) |
|---|---|
| 07-APR-2004 | GOM_CAL_AXVIEC20040406_084051_20040404_000000_20100101_000000 (Orbit 10974, date 05-APR-2004) |
| 17-APR-2004 | GOM_CAL_AXVIEC20040416_131836_20040413_000000_20100101_000000 (orbit 11085, date 13-APR-2004) |
| 24-APR-2004 | GOM_CAL_AXVIEC20040423_075737_20040421_000000_20100101_000000 (orbit 11215, date 22-APR-2004) |

## *5.2 Quality Flags Monitoring*

In this section it is monitored some Product Quality information stored in the level 1b products that are not flagged (MPH error flag not set). The products flagged were around 0.9% of the products received during April for the quality monitoring.

On the one hand, for every product we have information of the **number of measurements** where a given problem was detected (i.e. number of invalid measurements, number of measurements containing saturated samples, number of measurements with demodulation flag set…). On the other hand, there are **flags** that indicate problems within the product (i.e. flag set to one if the reference spectrum was computed from DB, flag set to zero if SATU data were not used…).

For the information on the number of measurements a plot (percentages) is provided in fig. 5.2-1. It can be seen that the cosmic rays hits occurred often for the 95% of the measurements of the product. Another observation that can be done is that, for many products, the 30 % of the measurements have the star

signal falling outside the central band. The other values (% of invalid measurements per product, % of measurements per product with datation errors…) are quite low.

The flag information is given in table 5.2-1. It is reported also the percentage of the products that have at least one measurement with demodulation flag set.

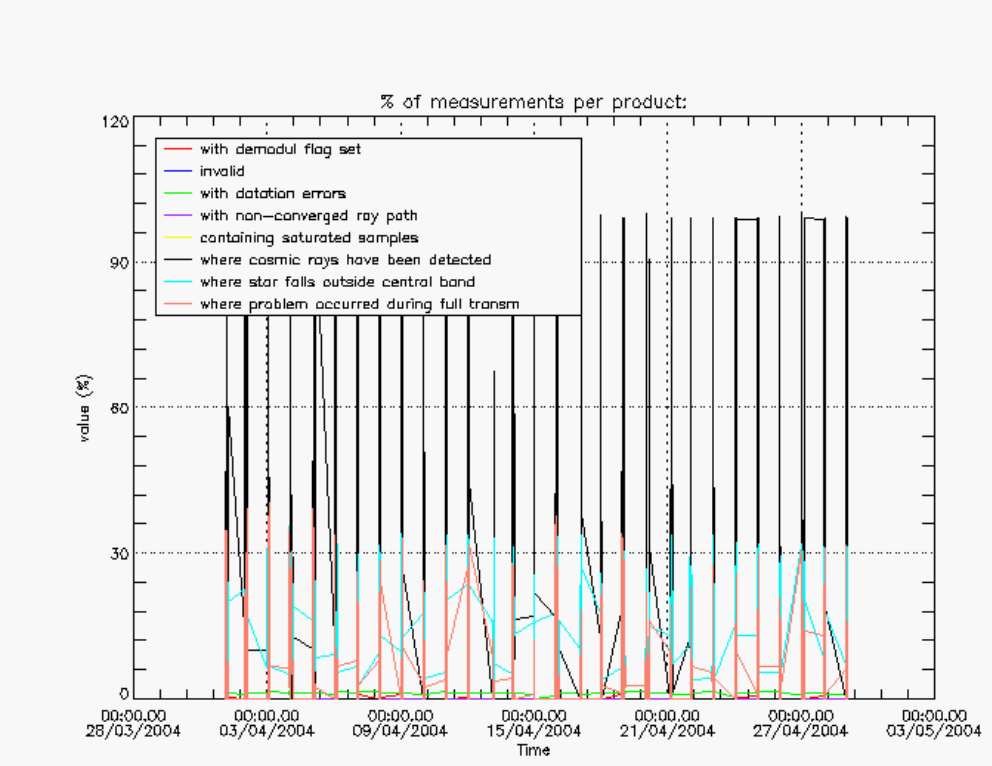


**Figure 5.2-1: Level 1b product quality monitoring**

**Table 5.2-1: Percentage of products during the reporting period with:**

| | |
|---|---|
| At least one measurement with demodulation flag set: | 14.600 % |
| Reference spectrum computed from DB: | 0.00000 % |
| Reference spectrum with small number of measurements: | 0.00000 % |
| SATU data not used: | 0.00000 % |

## *5.3 Spectral Performance*

A spectral calibration has been performed during April and again one of the values of the spectral shifts performed is above the warning threshold 0.07.

The values reported (table 5.3-1) are, for every star ID (1, 2, 4, 9, 18, 25), the wavelength of the first useful pixel of SPA2. This value is calculated by addition to the actual wavelength assignment, the spectral shift for which a maximum correlation has been found between the reference spectrum and the one of the occultation.

During the last wavelength calibration analysis performed using several occultations, the spectral shifts are 0.09 for star id number 1, 0.078 for star id number 2 and 0.072 for star id number 18 (see table 5.3-1). These shifts are greater than 0.07 (warning value) and QWG investigation has been initiated on March.

The star number 4 is left in table 5.3-1 even if the values of the wavelength are very different from the nominal one. It should be just kept in mind that the values of the shift should be always of the same order (~0.4) but this star will not be used for calibration purposes.

**Table 5.3-1: Wavelength assignment calculated for several occultations since November 2002**

| Star ID / Level 0 date | 1 | 2 | 4 | 9 | 18 | 25 |
|---|---|---|---|---|---|---|
| **20021112_062935** | Occ.30: 690.455750 | Occ.26: 690.458740 | | Occ.28: 690.492981 | | |
| **20021219_102754** | | Occ.33: 690.468140 | Occ.26: 690.875122 | | | |
| **20030101_151630** | Occ.3: 690.445068 | Occ.37: 690.466003 | Occ.30: 690.878540 | | | |
| **20030110_121504** | | Occ.32: 690.465088 | Occ.25: 690.882385 | | | |
| **20030201_090221** | | | | | | Occ.21: 690.492981 |
| **20030415_123156** | | | Occ.29: 690.959534 | | Occ.20: 690.552002 | Occ.28: 690.492981 |
| **20030419_170041** | | | Occ.29: 690.957520 | | Occ.23: 690.555420 | |
| **20030428_072600** | | | | | Occ.19: 690.553645 | Occ.28: 690. 492981 |
| **20030717_053233** | | | | Occ. 22: 690.473816 | Occ. 26: 690.446594 | |
| **20040123_091615** | Occ.1: 690.400513 Occ.40: 690.401550 | Occ.35: 690.415161 | Occ.27: 690.852478 | | | |
| **20040222_065917** | | | Occ.25: 690. 850830 | | | Occ.21: 690. 492981 |
| **20040128_163559** | Occ.3: 690.399414 | | | | | Occ.23: 690. 492981 |
| **20040404_012642** | | | Occ 28: 690.890564 | | Occ 22: 690.492981 | |
| **20040404_081716** | | | Occ 26: 690.886963 | | Occ 19: 690.420593 | Occ 25: 690.492981 |

## *5.4 Radiometric Performance*

### 5.4.1 RADIOMETRIC SENSITIVITY

The monitoring performed consists in the calculation of the radiometric sensitivity of each CCD by computing the ratio between parts of the reference spectrum using specific stars. The parts of spectrum used are:

- UV: 250–300 nm
- Yellow: 500–550 nm
- Red: 640–690 nm
- Ir1: 761-770 nm
- Ir2: 935-944 nm

For the spectrometers the ratios are with respect to the 'yellow' spectral range. For the photometers, the ratio is calculated dividing the mean photometer signal above the atmosphere (115 km) by the 'yellow' spectral range (for PH1) or by the 'red' spectral range (for PH2).

The variation of the normalized ratio should be within a given threshold actually set to 10% (see table 5.4-1 that corresponds to fig. 5.4-1). For every star, this variation is calculated as the difference between the maximum (or minimum) ratio, and the mean over the 15 first values (if there are not 15 values computed yet, all values are used). Values outside the warning threshold of 10% are observed for the photometers, and investigations were performed at QWG. The star 18 has been studied in depth and two possible causes of these abnormal ratios are in place:

- The pointing azimuth of star 18 is going into the vignetting area during the period of the high peak, so the reference star spectrum used for the computation of the radiometric sensitivity ratio contains a contribution due to the vignetting correction. By looking at the UV and Red ratios of fig. 5.4-1, there is no high variation of the ratio, as the vignetting effect does not affect the SPA. For the IR1 and IR2 ratios the high variation seems to be due to some residual error in the vignetting correction.

- The difference between the SPA reference star spectra for orbits 08010 (azimuth 17.5 deg) and orbit 08428 (azimuth -9 deg) does not look like a star or the sun spectrum; it rather looks like the reflectivity correction curve.

A new reflectivity correction LUT is in use since 12$^{th}$ February 2004 and as it can be seen in fig. 5.4-2 and in table 5.4-2, the ratios for star number 4 and 25 are already outside the threshold. More investigations are needed on this issue.

**Table 5.4-1: Variation of RS for the different ratios (corresponds to fig.5.4-1). Should be less than 10%**

| Star Id | % Variation of UV ratio | % Variation of Red ratio | % Variation of IR1 ratio | % Variation of IR2 ratio | % Variation of Ph1 ratio | % Variation of Ph2 ratio |
|---|---|---|---|---|---|---|
| **1** | 0.543863 | 0.207967 | 0.401701 | 0.193903 | 8.55029 | 30.1656 |
| **2** | 0.158766 | 0.259793 | 0.625175 | 0.216532 | 4.52068 | 6.07233 |
| **4** | 0.106818 | 0.535285 | 1.17073 | 1.01193 | 8.08780 | 20.1837 |
| **9** | 1.69204 | 0.213861 | 0.364793 | 0.233455 | 4.79555 | 9.05862 |
| **18** | 0.447647 | 0.568593 | 0.844914 | 0.852089 | 14.7885 | 299.989 |
| **25** | 7.66627 | 0.551322 | 0.654513 | 1.12662 | 15.9214 | 78.6219 |

**Table 5.4-2: Variation of RS for the different ratios since the change in reflectivity LUT (corresponds to fig. 5.4-2)**

| Star Id | % Variation of UV ratio | % Variation of Red ratio | % Variation of IR1 ratio | % Variation of IR2 ratio | % Variation of Ph1 ratio | % Variation of Ph2 ratio |
|---|---|---|---|---|---|---|
| **4** | 0.151019 | 0.243592 | 0.326696 | 0.640467 | 7.21849 | 15.3352 |
| **18** | 0.304873 | 0.404969 | 0.744398 | 0.510854 | 0.919706 | 5.52472 |
| **25** | 4.88646 | 0.580084 | 0.604873 | 1.0409 | 6.45528 | 48.2979 |

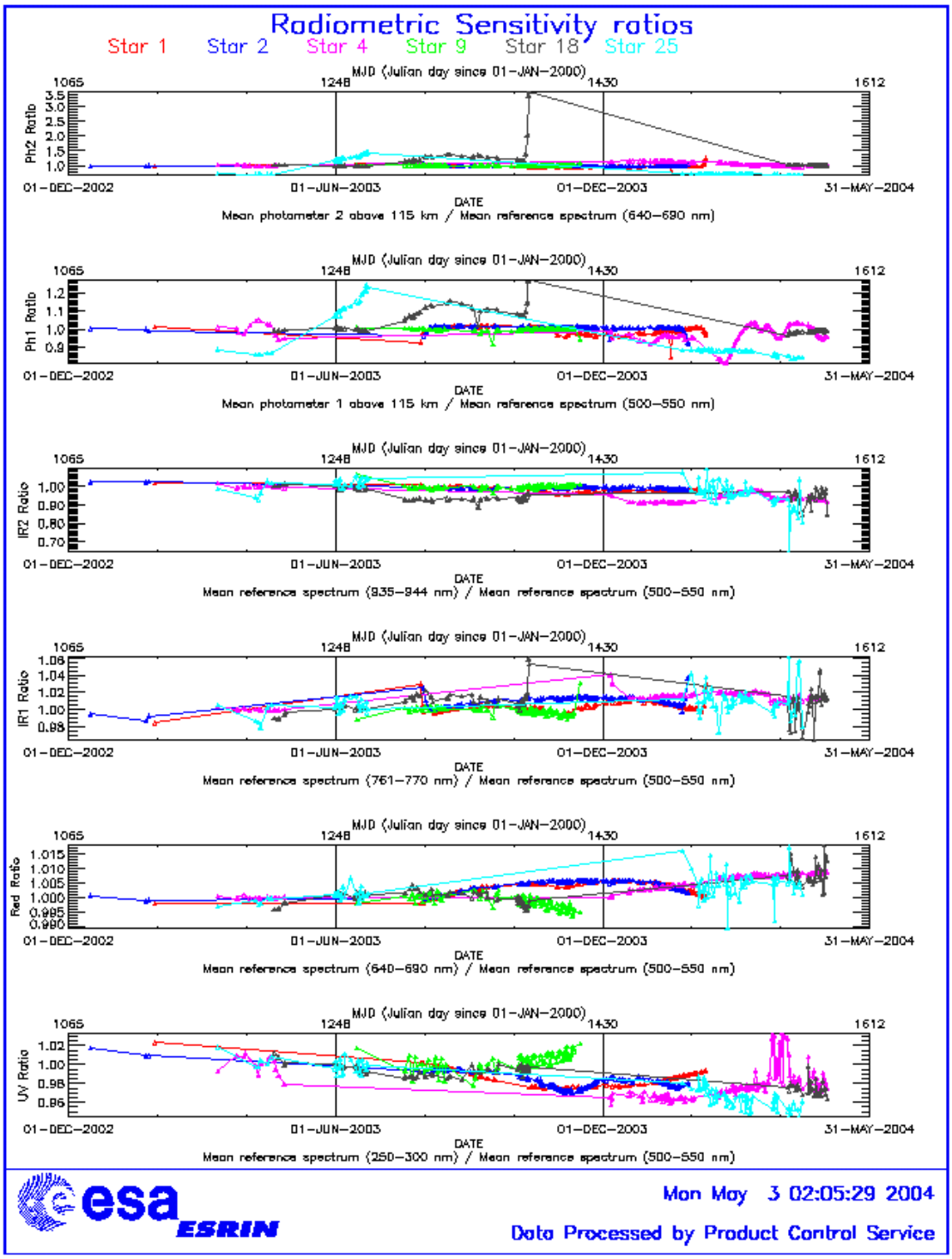


**Figure 5.4-1: Radiometric sensitivity ratios since December 2002**

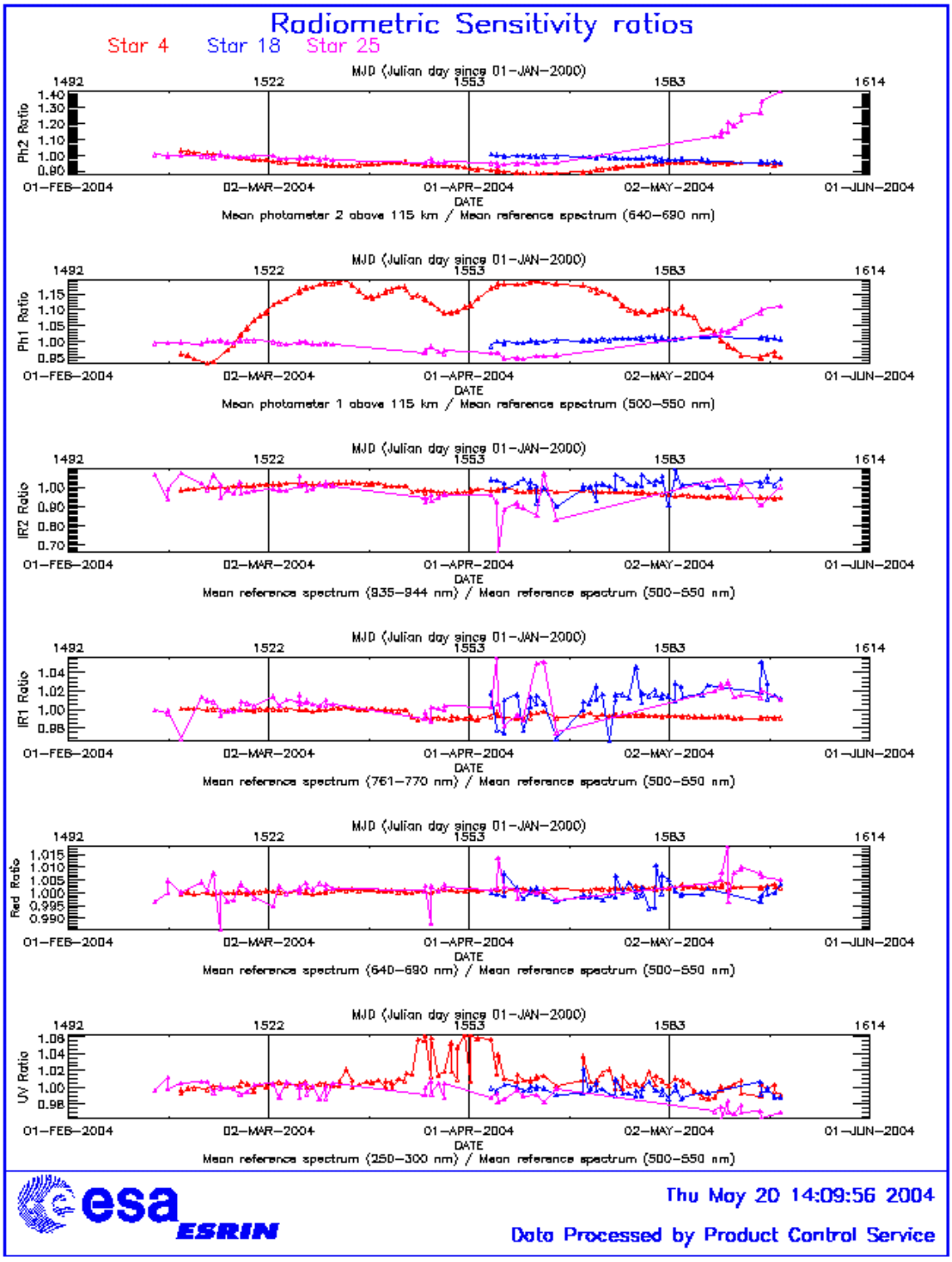


**Figure 5.4-2: Radiometric sensitivity ratios since the change in the Reflectivity LUT**

### 5.4.2 PIXEL RESPONSE NON UNIFORMITY

No new PRNU calibration has been done during the reporting month. During May 2003 a new PRNU calibration has been performed and processed into an update of the PRNU maps for the SPB1 and SPB2 that have been included in the auxiliary file GOM_CAL disseminated at the end of June 2003.

## *5.5 Other Calibration Results*

Future reports will address other calibration results, when available.

# 6 LEVEL 2 PRODUCT QUALITY MONITORING

## *6.1 Processor Configuration*

### 6.1.1 VERSION

No level 2 products from the operational ground segment have been disseminated during April to the users. About 80% of GOM_NL__2P products have been received in the PCF for routine quality control and long term trend monitoring. The current level 2-processor software version for the operational ground segment is GOMOS/4.02 (see table 6.1-1). The product specification is PO-RS-MDA-GS2009_10_3H. The improvements defined at the first Validation Workshop have been implemented into the prototype processor GOPR 6.0a (see table 6.1-2), before implementation into the operational one. In the mean time, Cal/Val teams are supplied with selected data sets generated by this prototype processor.

**Table 6.1-1: PDS level 2 product version and main modifications implemented**

| Date | Version | Description of changes |
|---|---|---|
| 23-MAR-2003 | Level 2 version 4.02 at PDHS-E and PDHS-K | Algorithm baseline level 2 DPM 5.5:<br><br>Section 3<br>• Add references to technical notes on Tikhonov regularization<br>• Change High level breakdown of modules: SMO/PFG<br>• Change parameter: NFS in l2 ADF<br>• Change parameter $\sigma_G$ in l2 ADF (Table 3.4.1.1-II)<br>• Change content of Level 2/res products - GAP<br>• Change time sampling discretisation<br>• Add covariance matrix explanation<br><br>Section 5<br>• Replace SMO by PFG VER-1/2: Depending on NFS, Apply either a Gaussian filter or a Tikhonov regularization to the vertical inversion |

| | | |
|---|---|---|
| | | matrix<br>• Unit conversion applied on kernel matrix<br>• Suppress VER-3<br><br>Section 6<br>• GOMOS Atmospheric Profile (GAP): not used in this version<br>• Time sampling in equation (6.5.3.7-73)<br>• See ref. [3] for more details |
| 31-MAY-2003 | Level 2 version 4.00 at PDHS-E and PDHS-K | Algorithm baseline level 2 DPM 5.4:<br>• Revision of some default values<br>• Add a new parameter<br>• Transmission model computation: suppress tests on valid pixels and species<br>• Apply a Gaussian filter to the vertical inversion matrix<br>• Very low signal values are substituted by threshold value<br>• See ref. [3] for more details |
| 21-NOV-2002 | Level 2 version 3.61 at PDHS-E and PDHS-K | Algorithm baseline level 2 DPM 5.3a:<br>• Revision of some default values<br>• Wording of test T11<br>• Dilution term computation of jend<br>• Covariance computation scaling applied before and after<br>• See ref. [3] for more details |

**Table 6.1-2: GOPR level 2 product version and main modifications implemented**

| Date | Version | Description of changes |
|---|---|---|
| 17-MAR-2004 | GOPR 6.0a | • Rename Turbulence MDS into High Resolution Temperature MDS (HRTP)<br>• Add vertical resolution per species in local densities MDS<br>• Add Solar zenith angle at tangent point and at satellite level in geolocation ADS<br>• Add "tangent point density from external model" in geolocation ADS<br>• Suppress contribution of "tangent point density from external model" in "local air density from GOMOS atmospheric profile" in geolocation ADS<br>(to be completed) |
| 18-AUG-2003 | GOPR 5.4d | • Tikhonov regularisation is implemented |
| 18-MAR-2003 | GOPR 5.4b | • Modification to implement the computation of Tmodel for spectrometer B (in version 5.4b, the Tmodel for SPB is still set to 1) |
| 30-JAN-2003 | GOPR 5.4a | • Modifications for ACRI internal use only. No impact on level 2 products. |

## 6.1.2 AUXILIARY DATA FILES (ADF)

The ADF's files in table 6.1-3 and 6.1-4 are used by the PDS to process the data from level 1 to level 2. For every type of file, the validity runs from the start validity time until the start validity time of the following one, but if an ADF file has been disseminated after the start validity time, it is obvious that it will be used by the PDS only after the dissemination time (this happens the majority of the times).

**Table 6.1-3: Table of historic GOM_PR2_AX files used by PDS for level 2 products generation**

| Used by PDS for Level 2 products generation in period | GOM_PR2_AX (GOMOS Processing level 2 configuration file) |
|---|---|
| 01-MAR-2002 → 29-JUL-2002 | GOM_PR2_AXVIEC20020121_165624_20020101_000000_20200101_000000<br>• Pre-launch configuration |
| 30-JUL-2002 → 02-SEP-2002 | GOM_PR2_AXVIEC20020729_083851_20020301_000000_20100101_000000<br>• Maximum value of chi2 before a warning flag is raised (set to 5)<br>• Maximum number of iterations for the main loop (set to 1) |
| 03-SEP-2002 → 12-NOV-2003 | GOM_PR2_AXVIEC20020902_151029_20020301_000000_20100101_000000<br>• Maximum value of chi2 before a warning flag is raised (set to 100) |
| 13-NOV-2003 | GOM_PR2_AXVIEC20021112_170458_20020301_000000_20100101_000000<br>• Smoothing mode<br>• Hanning filter<br>• Number of iterations<br>• Spectral windows to suppress the O2 absorption in the high spectral range of SPA2 |
| 23-MAR-2004<br>*Note*: this file was used by the GOMOS/4.02 processors before the IECF dissemination. The dissemination was done on 25th March 2004 | GOM_PR2_AXVIEC20040316_145613_20020301_000000_20100101_000000<br>• Pressure at the top of the atmosphere<br>• Number of GOMOS sources data (used in GAP)<br>• Activation flag for GOMOS sources data (GAP)<br>• Smoothing mode (after the spectral inversion)<br>• Atmosphere thickness |

**Table 6.1-4: Table of historic GOM_CRS_AX files used by PDS for level 2 products generation**

| Used by PDS for Level 2 products generation in period | GOM_CRS_AX (GOMOS Cross Sections file) |
|---|---|
| 01-MAR-2002 → 08-MAR-2002 | GOM_CRS_AXVIEC20020121_164026_20020101_000000_20200101_000000<br>• Pre-launch configuration |
| 09-MAR-2003 → 29-JUL-2002 | GOM_CRS_AXVIEC20020308_185417_20020101_000000_20200101_000000<br>• Corrected NUM_DSD in MPH - was 14 and is now 19 - and corrected spare DSD format by replacing last spare by carriage returns in file GOM_CRS_AXVIEC20020121_164026_20020101_000000_20200101_000000 |
| 30-JUL-2002 | GOM_CRS_AXVIEC20020729_082931_20020301_000000_20100101_000000<br>• O3 cross-sections summary description (SPA)<br>• NO3 cross-sections summary description<br>• O2 transmissions summary description<br>• H2O transmissions summary description<br>• O3 cross sections (SPA) |
| 26-MAR-2004<br>*Note*: the file was disseminated on 27 Jan 2004 but could not be used by PDS until version GOMOS/4.02 was in operation | GOM_CRS_AXVIEC20040127_150241_20020301_000000_20100101_000000<br>• Update of the O2 and H2O transmissions (S.A input)<br>• Extension by continuity of the O3 cross-section for SPB |

## 6.2 Other Level 2 Performance Issues

The plot presented in fig. 6.2-1 is the average of the Ozone values during April in a grid of 0.5 degrees in latitude per 1 km in altitude. Some known characteristics can be seen:

- $O_3$ concentrations show a decrease with latitude near 40 km altitude. In the lower latitudes $O_3$ is generated by photolysis of $O_2$
- In the middle stratosphere (25-30 km) $O_3$ is strongly influenced by transport effects. Strong meridional and zonal transport is visible in middle and higher latitudes
- The lower stratosphere shows an $O_3$ increase with latitude. Highest values can be found within the polar regions due to downward transport of rich air masses

Since the new version of GOMOS is in operation there has been an improvement in the Ozone values between 18 and 40 kilometres. Other characteristics seem not to be realistic as the values below 18 km where data are not reliable at the moment or some high values at –48 degrees latitude at high altitude (issues currently under investigation).

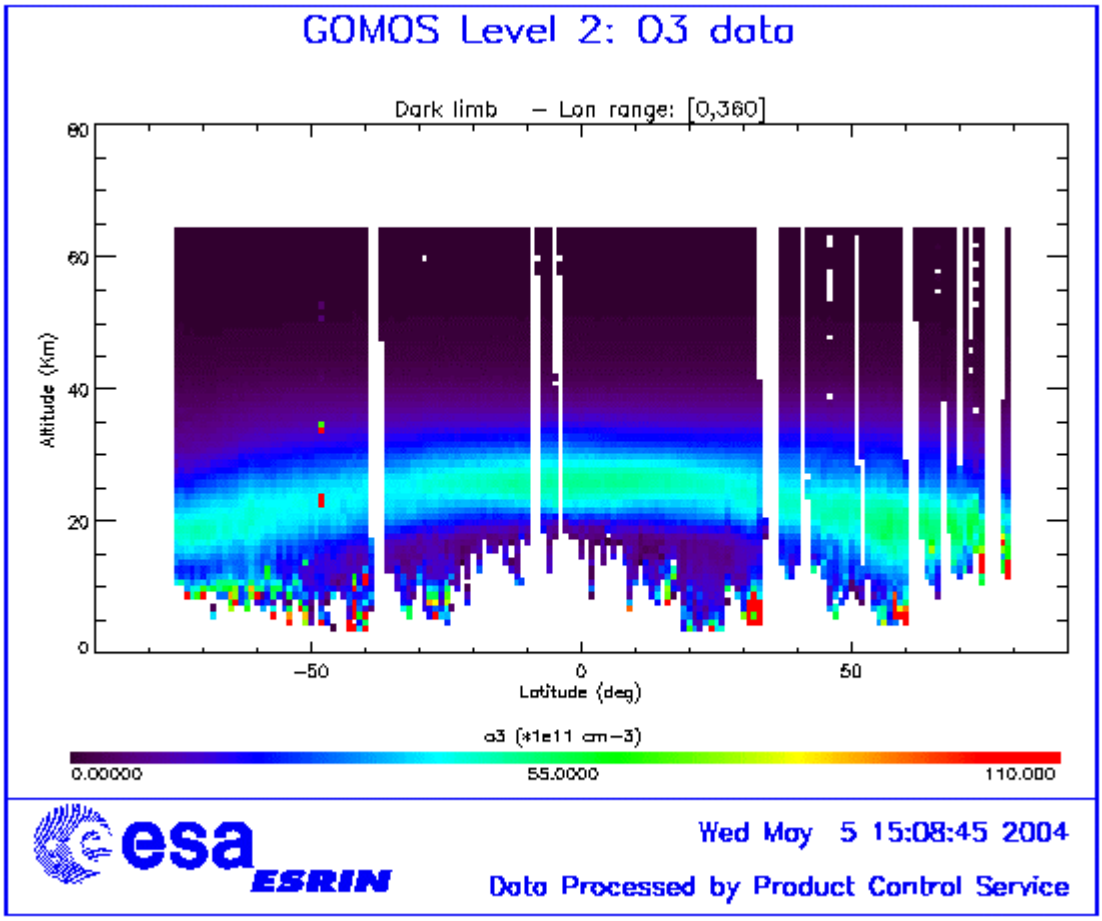


**Figure 6.2-1: Average GOMOS $O_3$ profile during April: average in a grid of 0.5° latitude x 1 km altitude**

# 7 VALIDATION ACTIVITIES AND RESULTS

The occultations of cycle 019 have been reprocessed by ACRI-ST as part as the full reprocessing of all GOMOS measurements. The processor version is v6.0a (future IPF version 5.0), which includes Tikhonov regularisation and Global DOAS Inversion on $NO_2$ and $NO_3$. For each altitude level, the local density value (of $O_3$, $NO_2$, $NO_3$, $O_2$, $H_2O$) is considered to be "valid" when its associated PCD flag is set to 0.

## *7.1 Inter-comparison with External Data*

Detailed inter-comparison results are available on http://envisat.esa.int/workshops/acve2

## *7.2 GOMOS-Climatology Comparisons*

Results will be presented upon availability.

## *7.3 GOMOS Assimilation*

This section presents the results of the work performed in the frame of the ACVT that have been shown at the validation workshop in Frascati on May 6th, 2004. Assimilation techniques may be used in two ways for validating measurements:

- It allows to extend the number of coincidences with independent measurements as the assimilated field may be viewed as an interpolation in space and time of the measurements to be validated
- It provides a framework for statistically analyzing the differences between the observations and the model forecasts that bring useful insights on both the measurements and observation error.

This study focused on measurements performed in August 2003, as a sufficient number of measurements were available in the validation dataset. Criteria have been applied in order to select local density measurements that are suitable for assimilation as well as for removing outliers. Thus the profile is kept if:

- The verticality is lower than 30° (only nearly vertical occultation are then considered, as it turned out that they were those that are less noisy). This value is given in the product as the field VERT_OCC in the NL_SUMMARY_QUALITY GADS, new parameter in the reprocessed data).
- The illumination condition is different of “bright limb”.

On a given profile, the only considered measurements are those for which:

- The PCD flag is 0
- The estimated standard deviation as given in the product is less than 10%
- The altitude is greater or equal to the altitude for which the ratio between the signal in the upper band and the signal in the central band is lower than 25% (given in the product as the flag NFI1 of the NL_SUMMARY_QUALITY GADS, new parameter in the reprocessed data).

Possible remaining outliers are then removed from the resulting profile by excluding points for which the relative fluctuation (with respect to the smoothed profile) is greater that 10%.

The fig. 7.3-1 shows the location of the selected GOMOS measurements during that period. The colors are relative to the illumination conditions (black: dark limb, green: straylight, blue: twilight). On the figure GOMOS particular observing pattern is apparent: a given star is observed on each orbit at the same latitude but shifted in longitude thus sampling circles of latitude. Areas without measurements are mainly the result of profiles removal by application of the selection criteria.

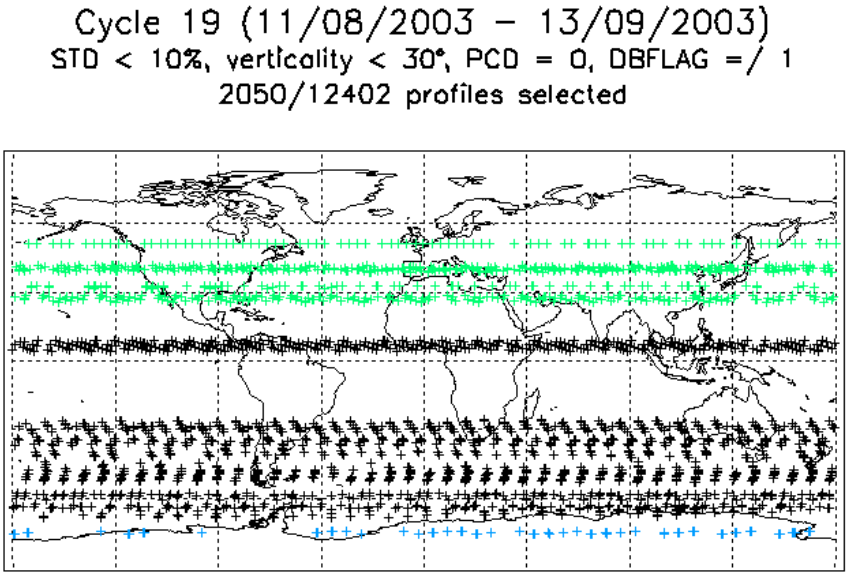


**Figure 7.3-1: GOMOS measurements for cycle 19. Colors means, black: dark limb, green: straylight, blue: twilight**

The aspect of these selected local density profiles (in mixing ratio; ECMWF temperature and pressure available in the GOMOS L2 products have been used to convert the concentrations given in the product) is shown on fig. 7.3-2: the overall shape appears to be reasonable with almost no outliers except in around 40 km for occultations affected by straylight. Note that all the measurements referred to as "twilight" in the middle stratosphere have been rejected.

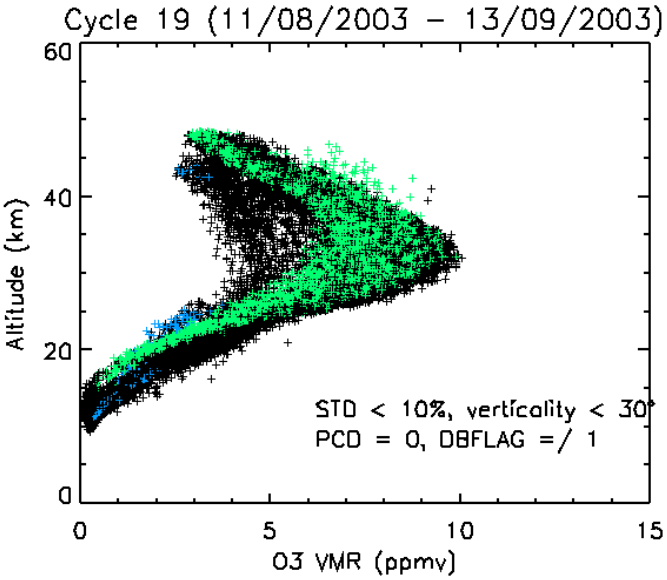


**Figure 7.3-2: local density profiles (in mixing ratio; ECMWF temperature and pressure available in the GOMOS L2 products have been used to convert the concentrations given in the product)**

The value that have been retained for the selection criteria are somewhat arbitrary and their suitability are questionable. In particular, the rejection of measurements that have an error bar greater than 10 % removes a lot of points in the middle stratosphere that may produce artifacts in the assimilation process. At these levels, ozone values calculated by assimilation process are thus left untouched, whereas ozone values at adjacent levels where measurements passed the selection criteria are modified by the assimilation process. Further investigations on a larger dataset are needed to be able to draw definite conclusions on that point.

In fig. 7.3-3 a comparison of profiles from the assimilated field with lidar soundings at Lauder is shown. At the beginning and at the end of the assimilation period shows a fair agreement. Local maxima observed on the assimilated field near 30 km are probably one of the artifacts produced by the selection as mentioned above.

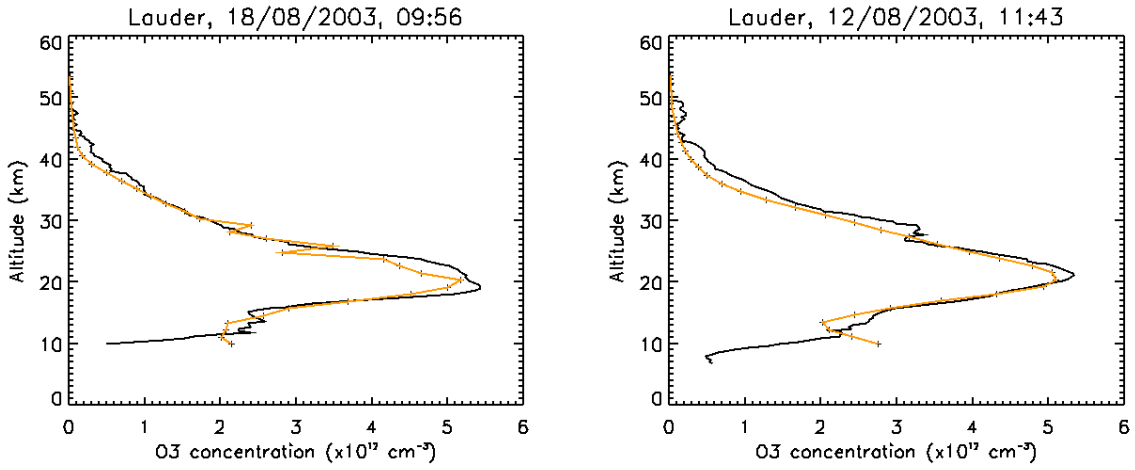


**Figure 7.3-3: Comparison with lidar soundings at Lauder. Lidar profile in black; assimilated one in orange**

Providing that a sufficient number of measurements are available, it is possible to compute the average difference between the assimilated field and the ground-based soundings. This provides a mean to evaluate the bias of the assimilated field. The fig. 7.3-4 shows this difference at 30 hPa (around 25 km) for the four stations of the southern hemisphere for which balloon soundings performed during the assimilation period are available on the NILU database (namely Belgrano, Dumont d'Urville, Lauder and Marambio). The value of the difference in mPa is indicated at the location of the station.

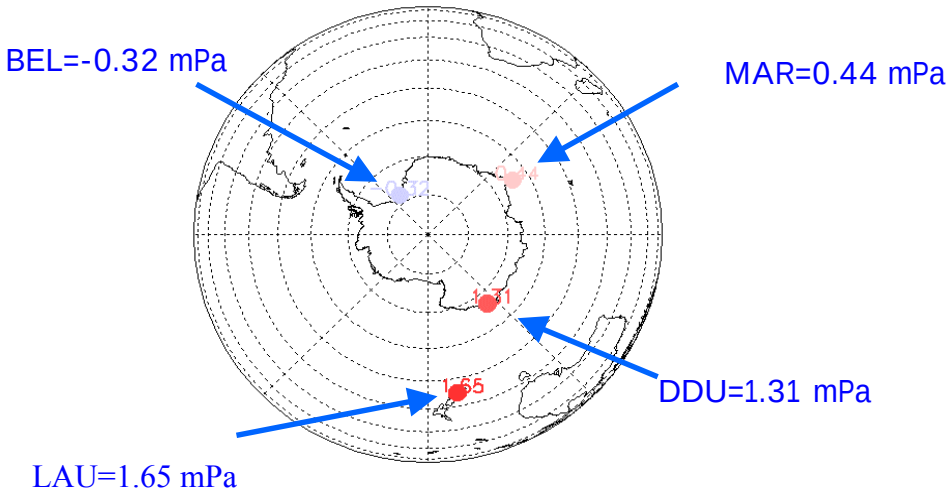


**Figure 7.3-4: difference between the assimilated field and the ground-based soundings**

Although it seems that the value of the difference tends to be larger as the latitude increases, there are not enough ground-based stations to conclude. The value of the bias of single inter-comparisons is comprised between –0.32 and 1.65 mPa that amounts to –6 up to 33 % (considering that the average value of ozone at that level is 5 mPa). Reducing the uncertainty interval will be possible by extending the assimilation period.

The other aspect of using assimilation for validation is to consider the differences between observations and forecasts (OmF) and observations and analyses (OmA). The fig.7.3-5 shows these differences for all the individual measurements that have been assimilated and for two layers in the low and in the middle stratosphere. Clearly apparent is the fact that the variability of the OmA is reduced with respect to the OmF for both levels indicating that the assimilation performs well. There seems to exist a linear increase of the average value of the OmF for the lowermost level. It is yet not clear whether this indicates a bias in the measurements.

The OmF can theoretically be used to statistically estimate the stationary properties of the measurements error (as well as of the model error). Indeed, the covariance of the OmF is the sum of the covariance of the model error and of the covariance of the instrumental error:

$$\mathrm{cov}(OmF) = \mathrm{cov}(E_{meas}) + \mathrm{cov}(E_{mod})$$

So the variance of the OmF provides an upper limit for the instrumental error. This value is shown on fig. 7.3-6 for several layers as a profile of relative error. It appears that the instrumental precision is of the order of 5 % in the range 30-40 km, a value coherent with the estimations obtained by the GBMCD and ESABC groups. Note that this value has been obtained by mixing profiles from various stars and thus from various precision. Yet, the precision of GOMOS measurements depends strongly on the physical characteristics of the observed star. So it may well be that the precision of GOMOS ozone profiles obtained with weak stars is much higher. This value does not take into account that the precision may depends as well on the latitude.

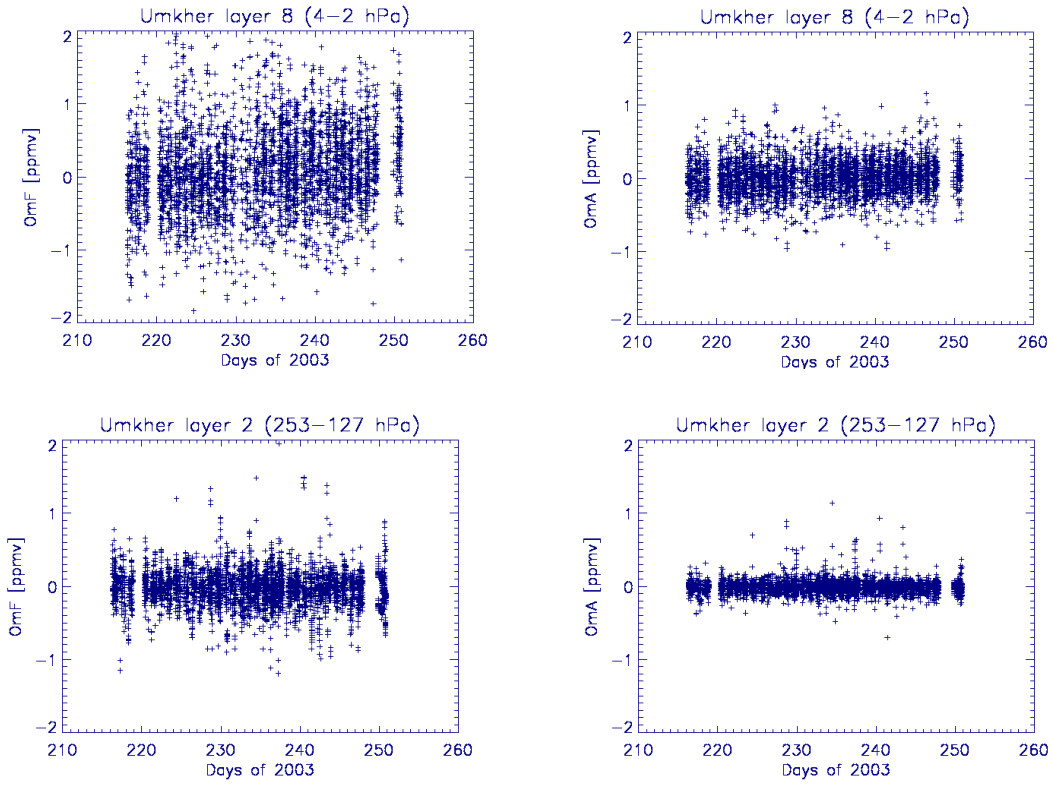


**Figure 7.3-5: Differences between observations and forecasts (OmF) and observations and analyses (OmA)**

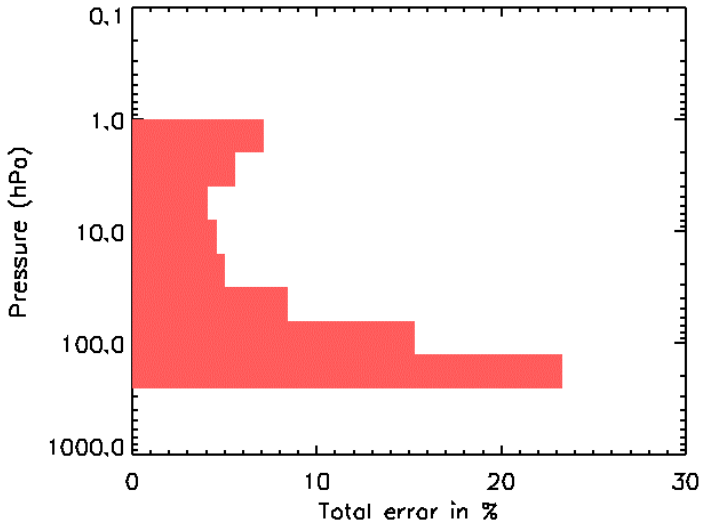


**Figure 7.3-6: Profile of relative error**

## *7.4 Consistency Verification: GOMOS-GOMOS Inter-comparison*

### 7.4.1 OZONE VERTICAL PROFILES

The vertical profiles of $O_3$ are plotted in fig. 7.4-1, per category of latitude, verticality, star magnitude and star temperature. As expected, there are less outliers for measurements at low latitudes than at other latitudes. No specific feature can be observed for other categories.

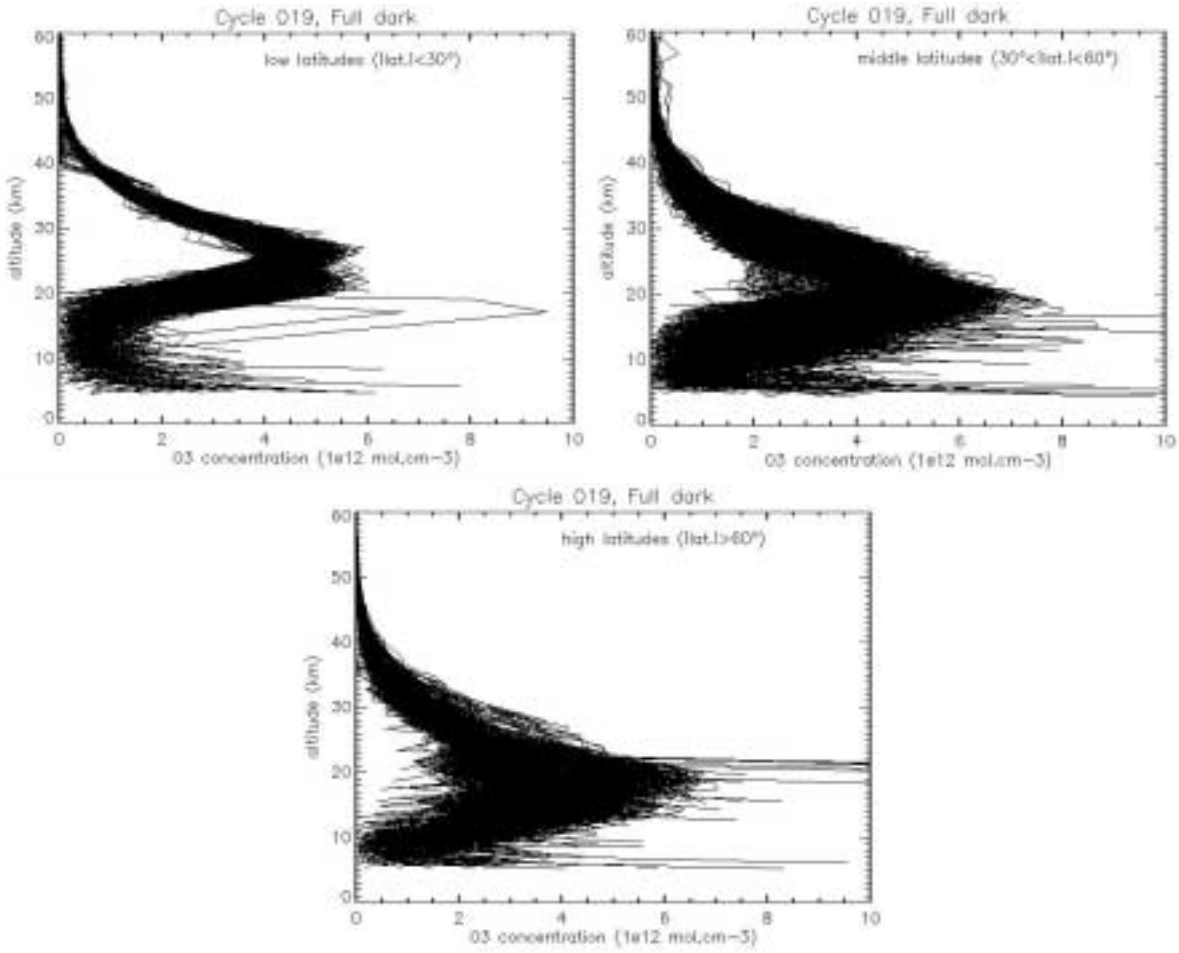


**Figure 7.4-1: Vertical profiles of $O_3$ concentration as a function of altitude, for different latitude ranges, for full dark illumination conditions**

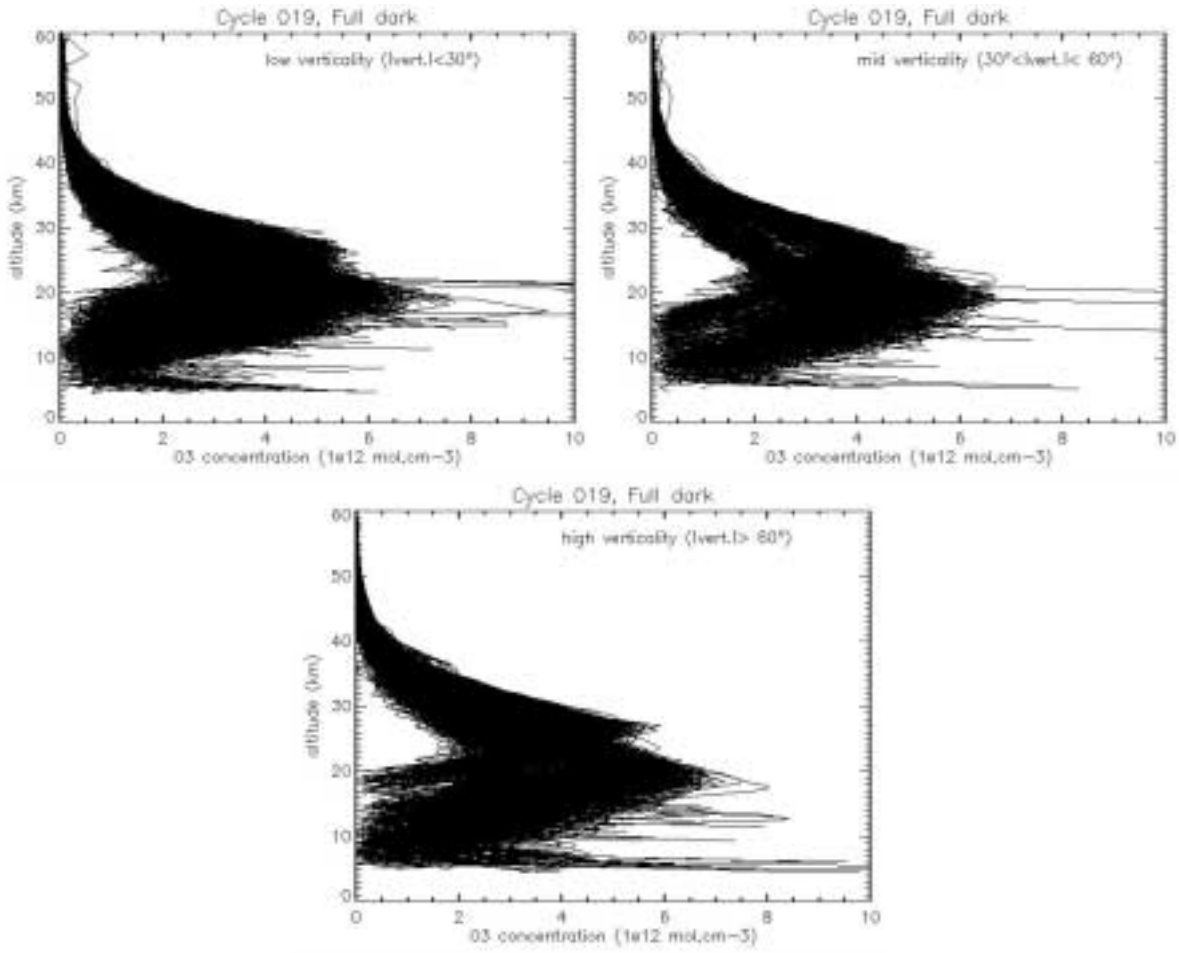


**Figure 7.4-2: Vertical profiles of $O_3$ concentration as a function of altitude, for different verticality ranges, for full dark illumination conditions**

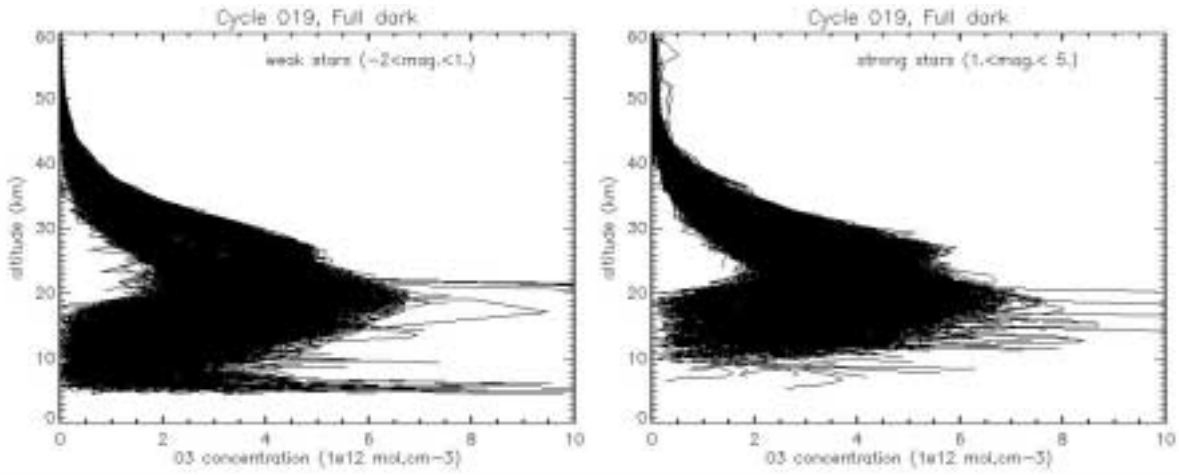


**Figure 7.4-3: Vertical profiles of $O_3$ concentration as a function of altitude, for different ranges of star magnitude, for full dark illumination conditions**

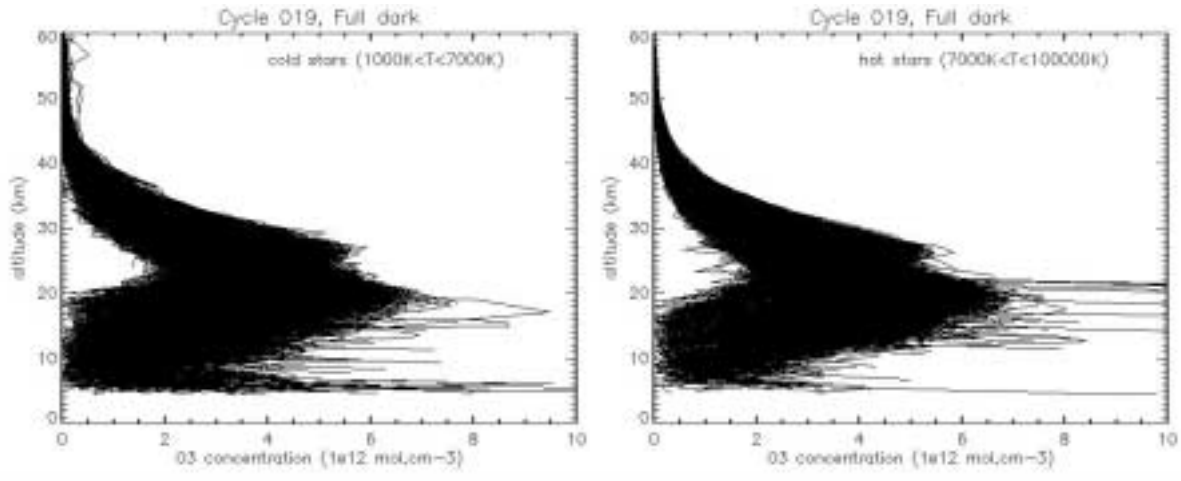


**Figure 7.4-4: Vertical profiles of $O_3$ concentration as a function of altitude, for different ranges of star temperature, for full dark illumination conditions.**

## 7.4.2 AIR DENSITY AND $O_2$ VERTICAL PROFILES

Fig. 7.4-5 illustrates the correlation between values of GOMOS air density and values of ECMWF air density, for altitudes between 25km and 35km. The correlation is good, with a correlation coefficient equal to 0.91. This correlation remains good, when calculated with values at altitude levels between 20km and 30km (Fig. 7.4-6; correlation coefficient of 0.92).

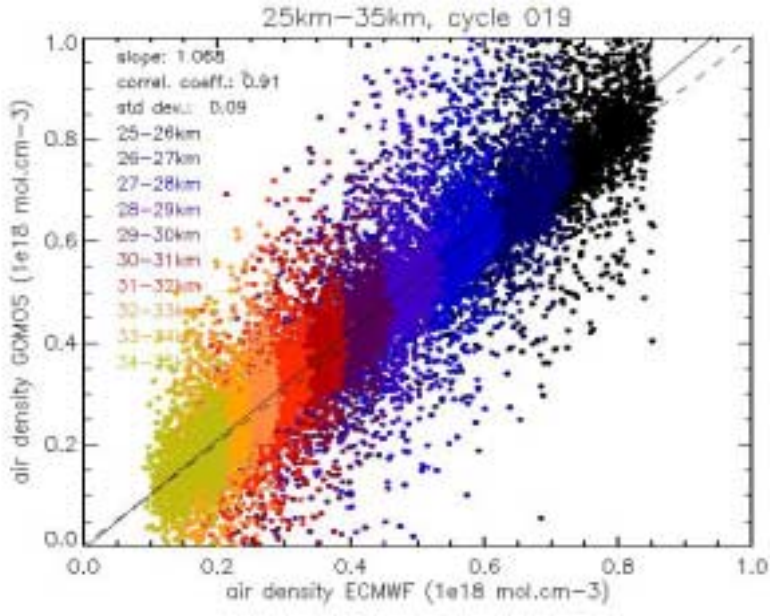


**Figure 7.4-5: Correlation between values of GOMOS air density and values of ECMWF air density, for altitudes between 25km and 35km, measured for cycle 019. The solid line plots the linear fit to the data**

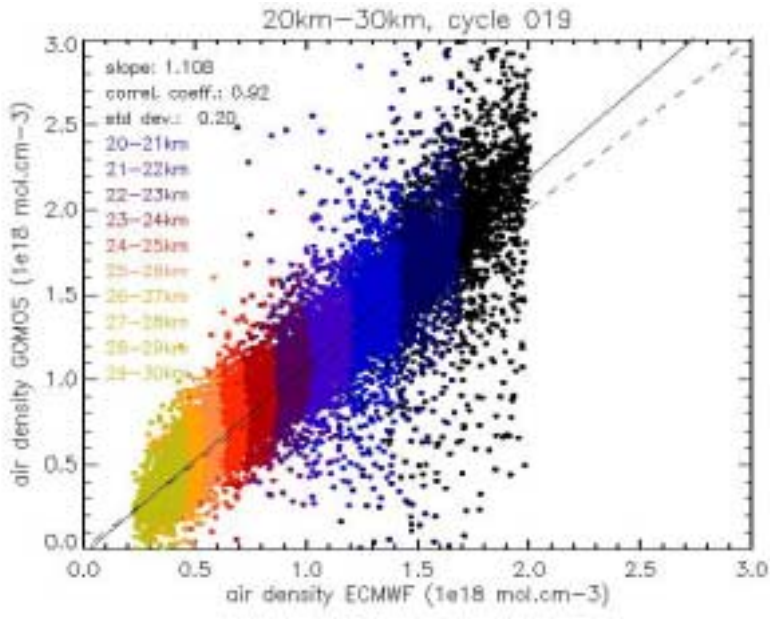


**Figure 7.4-6: Correlation between values of GOMOS air density and values of ECMWF air density, for altitudes between 20km and 30km, measured for cycle 019. The solid line plots the linear fit to the data**

Fig. 7.4-7 illustrates the correlation between values of GOMOS $O_2$ concentration and values of ECMWF $O_2$ concentration, for altitudes between 25km and 35km. The ECMWF $O_2$ vertical profile is reconstructed as 0.21 * ECMWF air density profile. The low correlation calculated between the two quantities in this case (correlation coefficient of 0.24) has been previously observed on similar datasets encompassing measurements at all latitudes. It is probably due to some specific profiles, and this will be further investigated.

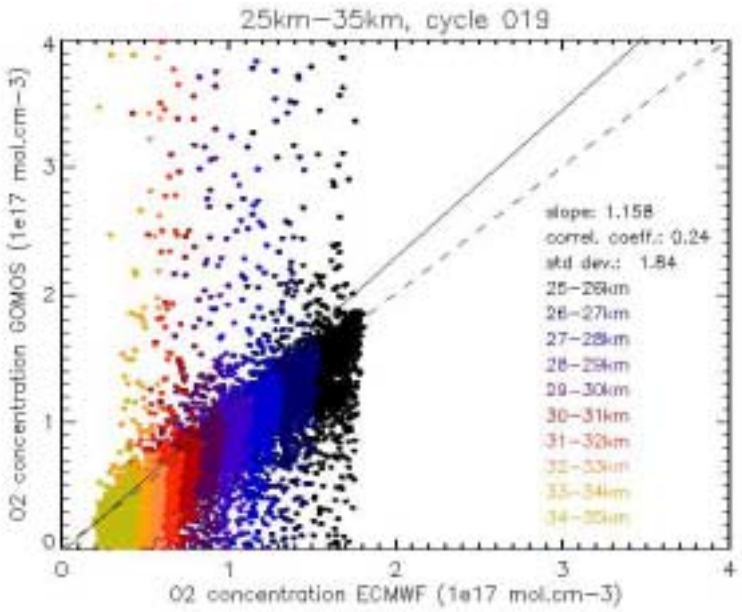


**Figure 7.4-7: Correlation between values of GOMOS $O_2$ concentration and values of ECMWF $O_2$ concentration, for altitudes between 25km and 35km, measured for cycle 019. The solid line plots the linear fit to the data**

Fig. 7.4-8 illustrates the correlation between values of GOMOS $O_2$ concentration and values of GOMOS $O_2$ concentration reconstructed as 0.21 * GOMOS air density profile, for altitudes between 25km and 35km. As for the previous figure, the high variability of $O_2$ GOMOS values for specific profiles is associated to a low correlation coefficient (0.20).

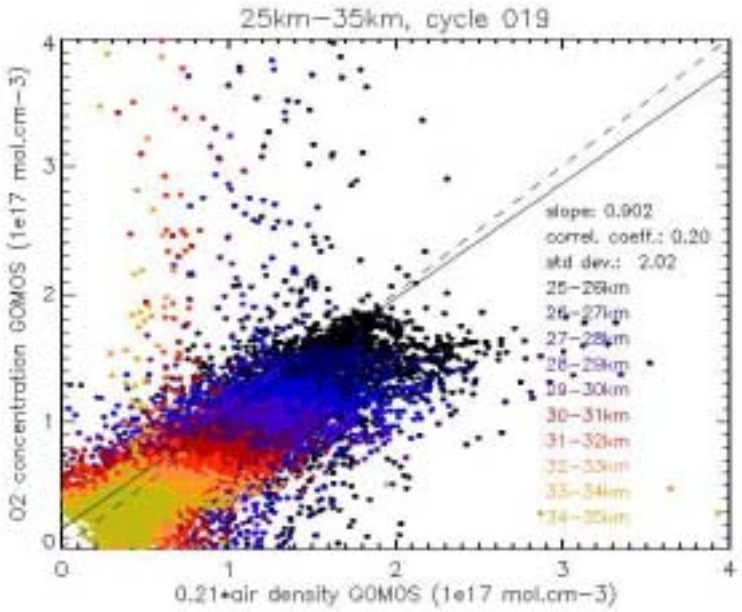


**Figure 7.4-8: Correlation between values of GOMOS $O_2$ concentration and values of GOMOS $O_2$ concentration calculated as 0.21* GOMOS air density profile, for altitudes between 25km and 35km, measured for cycle 019. The solid line plots the linear fit to the data**